MONOLAYER-THICK LIGHT-SENSITIVE NANOCRYSTAL SKINS OF ORIENTED COLLOIDAL QUANTUM WELLS

A Thesis Submitted to The Graduate School of Engineering and Science of Bilkent University in partial fulfillment of the requirements for
the degree of
Master of Science
in
Materials Science and Nanotechnology

by
Taylan Bozkaya

May 2023

MONOLAYER-THICK LIGHT-SENSITIVE NANOCRYSTAL SKINS OF ORIENTED COLLOIDAL QUANTUM WELLS

By Taylan Bozkaya

May 2023

We certify that we have read this thesis and that in our opinion it is fully adequate, in scope and in quality, as a thesis for degree of Master of Science

Hilmi Volkan Demir (Advisor)

Onur Tokel

Nihan Kosku Perkgöz

Approved for the Graduation School of Engineering and Science

Orhan Arıkan

Director of the Graduate School

ABSTRACT

LIGHT-SENSITIVE MONOLAYER-THICK NANOCRYSTAL SKINS OF ORIENTED COLLOIDAL QUANTUM WELLS

Taylan Bozkaya

M.S. in Materials Science and Nanotechnology

Advisor: Hilmi Volkan Demir

May 2023

Colloidal quantum wells (CQWs), a two-dimensional member of semiconductor nanocrystals, featuring very tight vertical quantum confinement, possess giant oscillator strengths. Also, CQWs exhibit remarkably large absorption cross-sections, thanks to their oscillator strengths combined with their laterally large geometries. Additionally, as a powerful tool of fabrication, CQWs lend themselves to be conveniently self-assembled into monolayer-thick films in a single orientation of our choice: either face-down (lying down on their large lateral surfaces and side by side leaving no large gap between them similar to a mosaic pattern) or edge-up (standing up on their thin edges and facing each other in a very dense superstructure formation of repeating chains). In this thesis, to make use of the attractive absorption properties of CQWs and leverage on our ability to construct their orientation-controlled self-assemblies, we show the first account of monolayer-thick light-sensitive nanocrystal skins (LS-NS) that employ self-oriented CQWs as their active absorptive layer. These CQW LS-NS devices operate on the principle of strong optical absorption of the monolayered assembly of CQWs and the subsequent photogenerated potential build-up across their strongly capacitive thin device for sensing in the visible to ultraviolet. Such oriented CQWs in the LS-NS device architecture yield profoundly reduced surface roughness in their monolayer-thick films, essential to high device performance. Here, specifically, we developed and demonstrated two groups of LS-NS devices: one group consisting of all face-down oriented CQWs and the other, of all edge-up ones. We systematically studied their photocharging effect, spectral sensitivity and decay times. We observed in all LS-NS devices that the

spectral sensitivity complies with the first (heavy-hole) and second (light hole) excitonic peaks of the absorption of the CQWs. We also found that, as the excitation power is increased, the peak photovoltage readout increases while the sensitivity decreases. The photocharging effect was further observed as the excitation was turned off. Finally, using the edge-up orientation, we identified a profound peak photovoltage signal enhancement. These findings of the thesis indicate that the proposed LS-NS devices of the orientation-controlled CQW monolayers hold great promise for applications in photos-sensing facades over larger surfaces.

Keywords: Nanocrystals, colloidal quantum wells (CQWs), light sensing, self-assembly, orientation-controlled film, monolayer film, nanofabrication.

ÖZET

TEK KATMAN KALINLIĞINDA YÖNLENDİRİLMİŞ KOLOİDAL KUANTUM KUYULARI TABANLI IŞIĞA DUYARLI NANOKRİSTAL YÜZEYLERİ

Taylan Bozkaya

Malzeme Bilimi ve Nanoteknoloji, Yüksek Lisans

Tez Danışmanı: Hilmi Volkan Demir

Mayıs 2023

Yarıiletken nanokristaller ailesinin iki-boyutlu üyesi olan koloidal kuantum kuyuları (KKK), dikey yönde kuantum sınırlaması ile yüksek osilatör gücüne sahip olan yapılarıyla dikkat çeker. Bunun yanı sıra, yatay yöndeki geniş geometrileri sayesinde dikkate değer derecede büyük soğurma kesitlerine sahiptirler. Ayrıca, güçlü bir fabrikasyon aracı olarak, KKK'lar tek katman kalınlığında yönel filmler olarak öz-dizilim yeteneği sunarlar. Yüz-aşağı (mozaik yapılara benzer, yanal yüzeyde geniş boşluk bırakmadan yan yana gelecek şekilde yatarak) ya da kenar-dik (ince kenarları üzerinde yüzeyleri birbirlerine bakan çok sıkı tekrar eden zincir üstyapılar halinde dikilerek). Bu tezde, KKKların yüksek soğurma özelliklerinden yararlanmak ve yönel-kontrollü öz-dizilimlerinden faydalanmak üzere, tek tabaka kalınlığında dizili KKK'lerin aktif soğurucu olarak kullanıldığı ışığa duyarlı nanokristal yüzeylerin ilk örneğini gösteriyoruz. Bu KKK tabanlı ışığa duyarlı kapasitif cihazlar, tek katmanlı öz-dizilime sahip KKK'ların güçlü optik soğurma özelliği ve foton soğurarak oluşan potansiyel fark birikimi sayesinde görünür ve morötesi bantta algılama yapmaktadır. Işığa duyarlı bu aygıtların mimarisinde, bahsetmiş olduğumuz tek katmanlı yönel öz-dizilimli KKK filmler sağladığı düşük yüzey pürüzlülüğü aygıt performansı için önemlidir. Burada KKK tabanlı ışığa duyarlı aygıtlar özellikle iki grup olarak geliştirmiş ve gösterilmiştir: Tümüyle yüz-aşağı ve tümüyle dik-kenar yönlendirilmiş KKK tabanlı ışığa duyarlı aygıtlar. Tüm bunlar ışığında sistematik olarak aygıtların

foto-yükleme etkisi, spektral duyarlılık ve yüksüzlenme süreleri üzerinde çalışılmıştır. Bu aygıtların spektral duyarlılıklarının KKK'ların birinci (ağır-elektron yokluğu) ve ikinci (hafif-elektron yokluğu) uyarılmış eksitonik soğrulma tepe noktaları ile uyum içerisinde olduğu gözlemlenmiştir. Bunun yanısıra uyarım gücü yükseldikçe, fotovoltaj tepe noktası yükselirken, aygıtların duyarlılıklarının azaldığı da gözlemlenmiştir. Foto-yükleme etkisi, uyarım kaynağı kapatıldığında da gözlemlenmeye devam edilmiştir. Son olarak kenar-dik yöneliminden faydalanılarak, fotovoltaj sinyal tepe noktasında güçlü bir iyileştirme kaydedilmiştir. Tezin bütün bu bulguları göstermektedir ki; tek katman kalınlığında yönlendirilmiş koloidal kuantum kuyuları tabanlı ışığa duyarlı nanokristal yüzeyleri, geniş alanlarda foton algılama uygulamalarında büyük bir gelecek vaad etmektedir.

Anahtar sözcükler: Nanokristaller, koloidal kuantum kuyuları, ışığı algılama, öz-dizilim, yönel-kontrollü film, tek tabaka film, nano fabrikasyon.

Acknowledgment

Firstly, I would like to present my gratitude to Prof. Hilmi Volkan Demir for all support during my study. Throughout my thesis work, I have learned great things from my supervisor who is a complete leader and really decent teacher.

I would like to acknowledge and want to thank all the technical and administrative staff of UNAM for providing us with a wonderful environment where I could complete my scientific works in the most perfect way.

I would also thank all my group members from Demir Research Group for a friendly working environment and for their team work. My special thanks go to Dr. Savaş Delikanlı and Furkan Işık, who have always helped and motivated me during my study. I also thank Özgün Akyüz, Emre Ünal, Rabia Önen, Dr. Betül Canımkurbey, Dr. Mohammed A. Ibrahem, Dr. Zeynep Dikmen, Rabia Önen, Dr. Tatiana Lastovina, Dr. Aysan Khaligh Vazirabadi, Dr. Zahra Adelpour, Dr. Mojtaba Sadeghi, Farzan Shabani, Rumon Miah, Furkan Şahin, Ahmet Tarık Işık, Anıl Çağrı Atak, İlayda Özkan, Tuğba Karahan, Taha Haddadi, Mohsin Waris, and Tevfik Bülent Kanmaz. I will never forget the times we spent together, for both our studies and all good times.

Finally, my special gratitudes go to my wife. I am really grateful for her all help and support during my thesis studies.

CONTENTS

List of Figures

List of Tables

Chapter 1

INTRODUCTION

Optical imaging, sensing, and telecommunication technologies are enabled by the detection of photons. For optical detection, incident photons must first be absorbed by a photosensitive material, and subsequently conversion of the incident optical signal as the input into an electrical signal as the output is necessary. For semiconductors, if the incident photon is at a larger photon energy than the bandgap energy of the semiconductor material, it is absorbed and converted into a bound pair of electron and hole, which is known as an exciton. This electron-hole pair can be separated and collected as free-carriers to generate the electrical output. By exploiting this concept in different ways, we may detect optical signals, convert them to electrical signals, and characterize the spectral flux of incident photons and time of optical illumination [1]**.**

Historically light detection has been shown by using crystal semiconductor-based and epitaxially grown photodetectors [1, 2]. Throughout the last few decades, c-Si and GaAs/AlGaAs, have been widely exhibited for different spectral windows of the photodetector technologies for numerous photo-sensing applications [3, 4]. Even though epitaxially grown or crystalline photodetectors offer quite a low noise-to-signal ratio relative to the rest of the photodetection approaches, they still have many limitations [5]. The first is due to the implemented material's spectral absorption profile being limited. Since those are bulk materials, they offer quite a small room for the bandgap variation. They perform best near the cutoff value of the material spectrally and suffer from diminished absorption beyond that region [6].

Additionally, most of those semiconductor materials are either grown by the Czochralski method and cut into substrates or epitaxially grown on top of the crystal substrates. Their production consumes too much energy. Since the Czochralski growth relies on melting of the starting raw material, and slowly cooling down for crystalline growth, this process requires too much energy [7]. On the other hand, epitaxial growth methods typically need high vacuum, substrate heating and/or plasma applications, ending up with high energy-consumption. Moreover, the need for high precision in their fabrication processes makes their resulting devices much more susceptible to fabrication malfunctions [8].

In recent years, colloidal quantum wells (CQWs), a member of the quasi-two-dimensional sub-family of semiconductor nanocrystals (NCs), have been exhibiting an increasing trend of interest for use in optoelectronic devices. CQWs offer attractive advantages including low fabrication cost (since they are solution-processable) and ease of application as a thin film by utilizing simple methods like spin-coating and self-assembly [9, 10, 11]. In addition, CQWs provide superior optical properties since they possess a well-defined vertical thickness of a few monolayers (MLs), resulting in a giant oscillator strength. Additionally, they have remarkably large absorption cross-sections [12]. They are also customizable in terms of absorption spectrum by adjusting the number of their monolayers. CQWs may consist of (4.5 ML, 5.5 ML, 6.5 ML…), which allows one to tune the absorption spectrum of their device just by controlling and tuning the number of their monolayers.

In this thesis work, our research interest mainly focuses on fabricating and demonstrating a novel class of light-sensitive nanocrystal-skins (LS-NS) made of such quasi-two-dimensional CQWs. NC skins offer an alternative architecture to current photosensitive devices [13]. As opposed to utilizing the photocurrent as a source of electrical output signal, LS-NS devices, they operate on the principle of photogenerated voltage build-up in the absence of either external bias or current. The basis of photovoltage build-up can be described as photo-induced capacitive polarization of the device near the metal-semiconductor contact thanks to the separation of electron-hole pairs in a transient state.

In this thesis, we introduce photosensors, photosensitivity, and mainstream photosensitive device structures, as well as wet-processed CQWs and their characteristics as an active layer of a photosensitive device. We also explain the operating principles of LS-NS devices briefly. In the remaining of this thesis, we briefly present the necessary knowledge for the thesis work. Specifically in Chapter 2, we briefly explain quantum confinement and discuss the implications of quantum confinement for semiconductor materials. Furthermore, we briefly explain the self-assembly technique and discuss the orientation-controlled self-assembly of 4.5 ML CdSe CQWs in particular. Next, we present the principles of photosensitivity and the two most common photosensitive semiconductor device architectures and their characteristics. Finally, we discuss the working principle and voltage-time profile of the LS-NS devices.

Next, in Chapter 3, we fabricate and demonstrate the first account of the light-sensitive monolayer-thick NC skins of orientation-controlled CQWs by utilizing their face-down oriented self-assembly. Here, we utilized commercial indium tin oxide-coated glass as the starting substrate of the device. Subsequently, we coated a thin layer of Al_2O_3 as the oxide layer. Using the self-assembly method, we deposited a monolayer of CdSe CQWs as the active layer and finally terminated the device with an aluminum layer. Following the device fabrication, we carried out a series of device characterizations and analytically expressed the voltage time behavior for the photovoltage build-up. While the absorption spectrum converges to a constant value, the spectral sensitivity of the resulting LS-NS device keeps rising. We reckon this behavior hints at the charge hopping mechanism for carriers while being transferred between metal-semiconductor contact.

In Chapter 4, we fabricate and demonstrate the light-sensitive monolayer-thick NC skins of the edge-up oriented CQWs by utilizing the method of edge-up self-assembly of CdSe CQWs for the first time. Here, we compared these devices with those fabricated with the spin-coated CQWs. In order to make an even comparison between those two, we optimized the spin-coated CQW film thickness to exhibit the same absorption level with the edge-up CQW devices. In this comparison we observed a significant amount

of enhancement on the peak voltage signal, which is nearly 8-fold stronger with respect to the control group of spin-coated CQW devices. We found these enhancements, for the sensitivity (and the decay times) of edge-up CQW devices, possibly resulting from the improvement in charge transfer because of the CQWs the orientation control most likely yielding a better contact between the metal and the edges of the edge-up oriented CQWs.

Chapter 2

SCIENTIFIC BACKGROUND

2.1 Quantum Confinement

When dealing with extremely small particles in terms of both mass and size, we start to observe unexpected behavior, which cannot explain or model using classical mechanics. For that, we need quantum mechanics. To explain this behavior (see Figure 2.1.1), we utilize Schrodinger's equation (Eq. **2.1.1)** and the discrete energy solutions (allowed energy states, E_n) to Schrodinger's equation (Eq. **2.1.2**).

$$-\frac{h^2}{2m}\frac{d^2\psi(x)}{d\ x^2} = E\psi \qquad \text{Eq. 2.1.1}$$

$$\mathbf{E_n} = \frac{h^2n^2}{8mL^2} \qquad \text{Eq. 2.1.2}$$

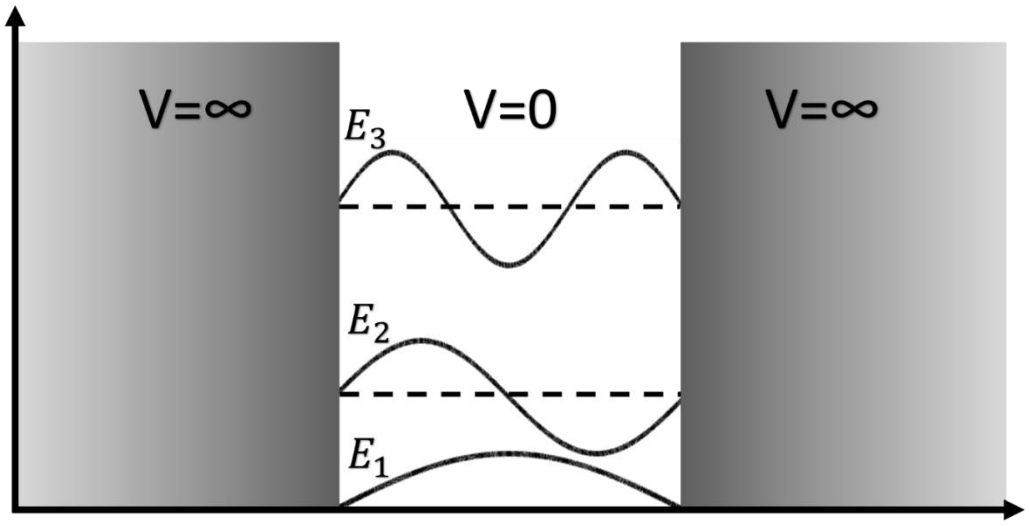

Figure 2.1.1 Illustration of infinite potential well with allowed energy states and corresponding wavefunctions.

If we scale down a piece of semiconductor material to a certain size in which the size of the material is comparable to the size of the exciton Bohr radius, we start to see effects of quantum confinement, which leads to discretization of the bands (E_n) and enlargement of the bandgap increased E_1 [14].

In Figure 2.1.2, we can see the illustration of a quantum well. As the distance between the two edges of the well is shortened, we start to observe a more pronounced quantum confinement effect. As the size shrinks, the available energy levels for the particle inside start to split further away (i.e., $\Delta E=(E_n-E_{n-1})$ increases).

We explain this effect via the solutions to Schrödinger equation (Eq. **2.1.1**) for a particle-in-a-box model. In Eq. **2.1.2**, E_n, is the eigen-energies of Eq. **2.1.1.** Energy eigenvalues depend on the particle's effective mass and the confined well's size. Since we deal with holes and electrons, their effective masses in the crystal lattice play an important role. Moreover, as the confinement is more and more pronounced, we can see that discrete energy levels are further separated, which may result in more than one transition for the recombination of electrons and holes.

If we discuss the effects of the confinement on the optical properties here, we can see that, as the confinement is more pronounced, we observe a blueshift in the emission/absorption spectra. Also, it is possible to see discrete peaks in the absorption spectrum due to split energy levels resulting from the confinement [14]**.**

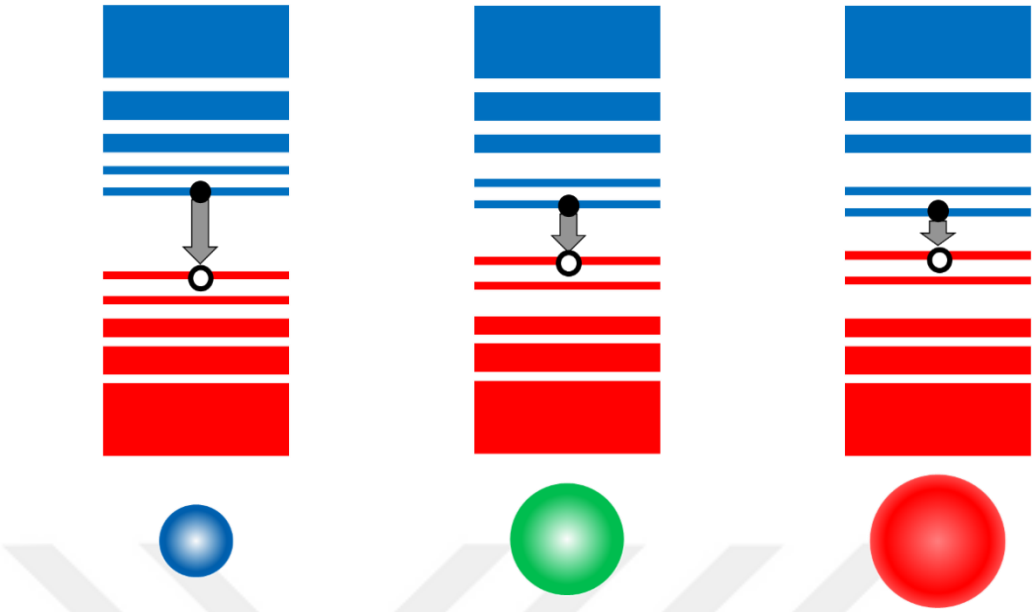

Figure 2.1.2 Quantum confinement effect in nanocrystals: Allowed energy levels depending on the size of nanocrystals.

Exciton Bohr radius is the spatial distance between the electron and hole in the excited phase. Even though the electron is excited, it is still bound to the hole as a pair with Coulombic interaction. Such energy is called exciton binding energy, and in that state the distance between the hole and electron is called the exciton Bohr radius. If the confinement through the crystal is comparable to this value, then the blue shift in the emission spectrum is more profound.

There are three dimensions to possibly confine a semiconductor crystal. Suppose we only confine the semiconductor in one dimension. In that case, it is called one-dimensional confinement; hence, this material is a quasi-2D material. We can give examples of many thin film devices, e.g., InGeS/InGe/InGeS thin film devices. It is also possible to confine semiconductor crystals along two dimensions, and those types of materials are classified as quasi-1D materials e.g., nanorods, which may be easily synthesized in solution. It is further possible to confine the crystal in all three dimensions. These are referred to as quasi-0D materials, e.g., quantum dots, which may be easily synthesized in solution like nanorods [14].

2.2 Colloidal Quantum Wells

Colloidal quantum wells are a quasi-two-dimensional family of semiconductor nanocrystals. They do not confine carriers in the horizontal plane due to large dimensions in that plane in the 10-50 nm range. However, due to their quasi-two-dimensional structure, they have well-defined thicknesses which can be controlled precisely at the atomic level in the crystal [15]. Therefore, strong quantum confinement of the nanocrystal is along its vertical dimension, the thickness. 4.5 and 5.5 monolayer thick CdSe nanocrystals are made of alternating Cd and Se crystal planes [15]. In a CdSe CQW nanocrystal, one of the faces permanently terminates with a layer of cadmium atoms, denoted as +0.5 monolayer. To clarify, there are four atomic layers of selenium and five atomic layers of cadmium in a 4.5 monolayer thick CdSe CQW.

Typical emission and absorption spectra of 4.5 ML CQWs are given in Figure 2.2.1. We can see a low-energy excitonic peak at 512 nm, denoted as the heavy-hole excitonic peak, and the second peak at 490nm, denoted as the light-hole peak (see Figure 2.2.1). The splitting of the excitonic peaks is because of the splitting of the conduction band resulting from different masses of the heavy hole and light hole [15]. The absorption profile of CdSe CQWs is similar to their epitaxially grown counterparts. Additionally, compared to the quantum dots, CQWs produce a much narrower emission bandwidth because of suppressed inhomogeneous broadening resulting from the well-defined thickness of the CQWs with a full-width-half-maximum (FWHM) typically in the range of 7-11 nm at room temperature.

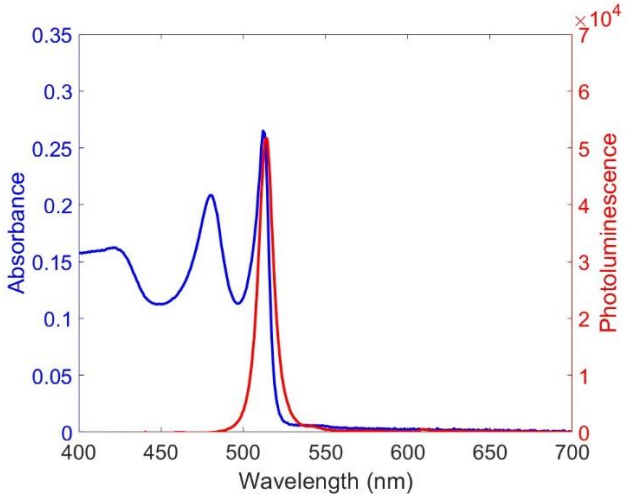

Figure 2.2.1 Absorption and emission spectra of 4.5 ML CdSe colloidal quantum wells.

Finally, the CQWs possess an uncommonly large absorption cross-section owing to their giant oscillator strength thanks to their very tight quantum confinement vertically and large cross-sectional area laterally [12]. These properties make CQWs an excellent candidate for photosensitive devices and photo-sensing applications.

2.3 Self-Assembly

In self-assembly, an unorganized and disordered system forms an organized and ordered structure by utilizing unit particles of the initial unorganized state as unit particles of the recursive organized system (see Figure 2.3.1). Self-assembly spontaneously happens without any external work. The self-assembly process can be described as a thermodynamic process in which there is an equilibrium between the unit constituents and the self-assembled ensembles. For the assembly of constituent molecules, rearrangement and reorganization of the molecules are expressed as the self-assembly of molecules. For such a process, specific interactions between molecules drive the self-assembly process. For such a process, determinant properties are the electrostatic, geometric, and photonic characteristics of the constituent molecules [16].

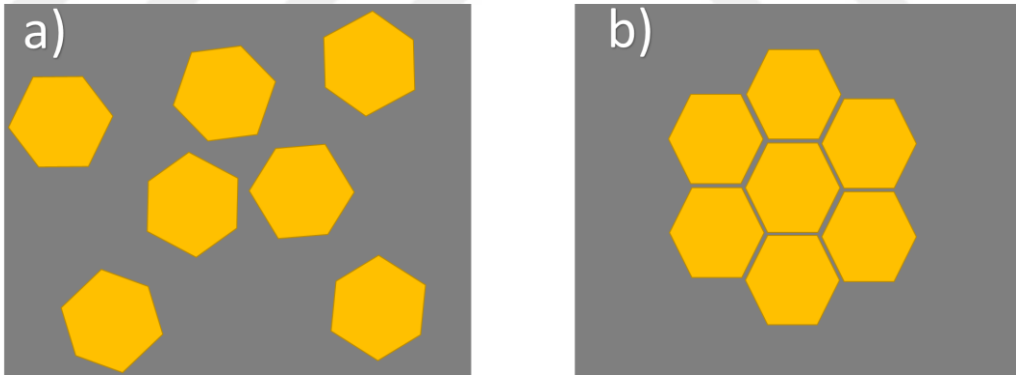

Figure 2.3.1 a) Distribution of the constituents in solution and b) self-assembled formation of the constituents.

Furthermore, the main driving forces for most self-assembly processes are weak intermolecular forces like hydrogen bonds, Vander Waals forces, and dipole-dipole interactions. The main reason behind this is the scale of particles we are dealing with; at such a small-scale external force like gravity becomes neglectable and weak interactions like intermolecular forces become dominant due to the reduced mass and

increased surface area of particles. Self-assembled constituents have a desirable low energy state than the isolated components. Therefore, it is a spontaneous thermodynamic process that tends to happen.

Why does self-assembly not happen all the time by itself? The answer to this question lies in the preset conditions. The self-assembled collection might be the most stable lowest energy state the constituents might be in; however, if we consider energy versus the distance between the constituents in Figure 2.3.2, there are many more stable states up until the lowest energy point in reached if the preset conditions are not set correctly. The evaporation of solvent or the change in the pH of the solution is not at a steady state or not slowly enough varying. The constituents may be stuck at those intermediate stable states. We might end up with a chaotic distribution of the constituent particles. Therefore, the rate of change in the conditions is one important figure of merit defining the final form of the self-assembled state of the constituent particles. As a result, the self-assembly is a bottom-up fabrication technique.

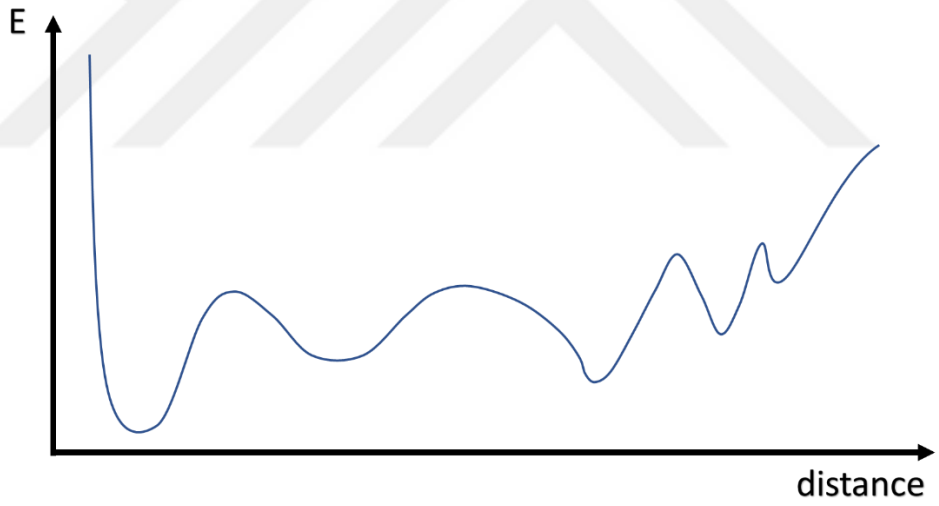

Figure 2.3.2 Energy versus distance for the constituents of self-assembly.

In this thesis, we utilize the self-assembly method to fabricate the required active thin film of the fabricated device of CQWS conformally and uniformly along the surface. Furthermore, we have the ability to set the necessary orientation of the nanoparticles CQWs by altering the polarity difference between the subphase and the solvent. Here we chose the method of evaporation for the self-assembly. As the evaporation of the solvent happens slowly, the colloidal quantum wells lose their colloidal stability.

Therefore, they gather to form the self-assembled monolayer film on top of the carefully selected subphase, which is immiscible with the solvent due to the polarity difference. The self-assembled film is laid down on top of the selected subphase. Here, acetonitrile was selected to form a face-down self-assembly (see Figure 2.3.3a). As the polarity difference between the CQWs and the subphase increases further, they start to repel each other and therefore, a film of edge-up colloidal quantum well (see Figure 2.3.3b) constitutes form on top of the subphase such as ethylene glycol [9] [10].

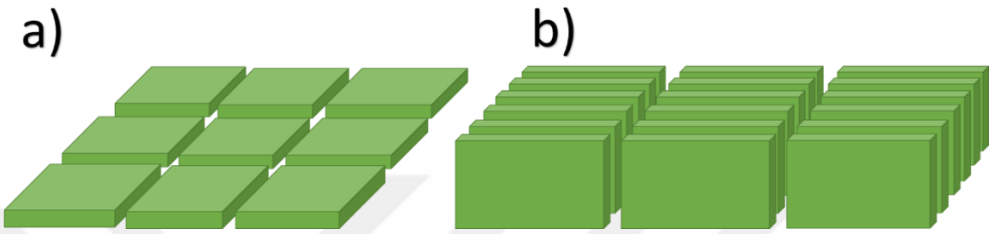

Figure 2.3.3 a) Face-down oriented self-assembly and b) edge-up oriented self-assembly of CQWs.

2.4 Fundamentals of Photosensitive Devices

Photosensing action in semiconductor-based photodetector devices relies on the photogeneration of electron-hole pairs. If the incident photon has an energy equal to or larger than the bandgap of the semiconductor material, then electrons are excited to the conduction band in which they can act like a free-carrier; similarly, the paired holes (which are the vacancy sites of the electrons and are thus relatively positively charged) can also move from one lattice site to another lattice site (see Figure 2.4.1). They also contribute to the current through the material as free-carriers. However, one needs to remember that holes and electrons have different effective masses and mobilities through the crystal lattice. There are two main ways to contribute current as a signal in a photosensitive semiconductor device conventionally.

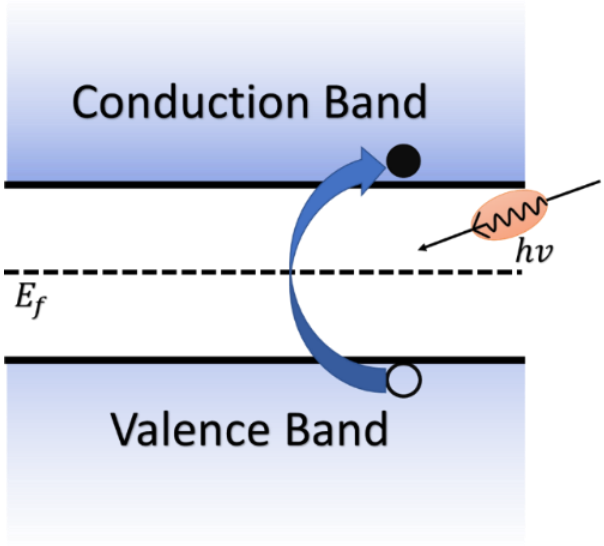

Figure 2.4.1 Photogeneration of an exciton in the semiconductor material.

Photoconductors: This type of device is a symmetric structure with two identical electrodes at either end and a piece of semiconductor between them (see Figure 2.4.2a). The primary phenomenon here is to keep the photoconductor under bias throughout the operation. Typically, at room temperature, there are thermally generated exciton pairs. Those electron-hole pairs also contribute to current passing through the device. However, suppose an incident beam has a photon energy larger than the bandgap of a semiconductor material or equal to it. In that case, this beam photogenerates electron-hole pairs in amount proportional to the intensity of the incident beam (see Figure 2.4.2b). Those photogenerated electrons and holes also contribute to the current and are proportional to the intensity of the incident light; therefore, it is called the photocurrent, which is larger than the dark current in magnitude under sufficient light exposure. This can also be thought of as if the incident light alters the resistance of the semiconductor material and, thus, under the constant bias a larger amount of current passes through the device (see Figure 2.4.2c) [17].

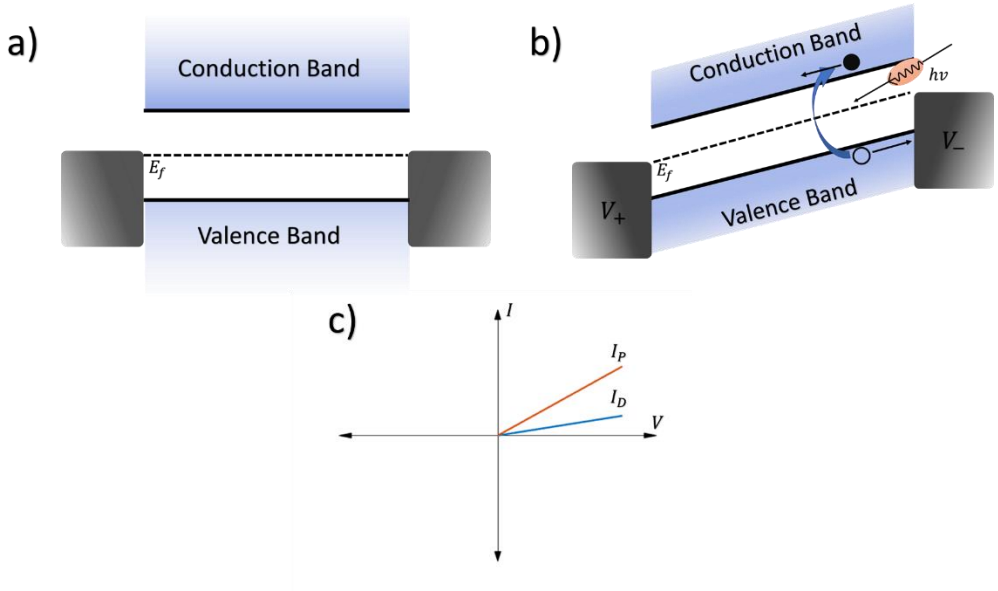

Figure 2.4.2 a) Band diagram of the metal-semiconductor-metal(M-S-M) photoconductor under no bias, b) band diagram of the M-S-M photoconductor under bias, and c) I-V characteristics of typical M-S-M device under dark and photoexcited conditions.

p-n or p-i-n photodiodes: These utilize the photosensitivity of semiconductor materials; however, this time, these devices are not symmetric, and they are diodes that pass the current through only one direction. More remarkably photodiodes provide photocurrent independent of the applied bias once they are sufficiently in the reverse bias mode (see Figure 2.4.3a). As you can also see in Figure 2.4.3b in the reverse bias region the photocurrent itself follows a nearly linear behavior proportional to incident optical power. This enables photocurrent to be generated depending on the excitation source. When an incident photon is absorbed in the junction's depletion region, it leads to the generation of an exciton, the bound electron-hole pair, which is separated by the built-in electric field in the depletion region. The electron separates from its pair, travels to the n-side, and is collected by the positively biased electrode. The hole separates from the pair and travels to the p-side, and the negatively biased electrode collects it. One should note that a nonzero current is running through the circuit under dark conditions, denoted as I_D which stands for dark current. There are multiple factors that determine the dark current; however, the source of the dark current is the nonzero temperatures. However, the dark current can be reduced if the system is cooled. Otherwise, thermal generation can cause considerably large noise for specific systems like mid-wave infrared photodetectors [18].

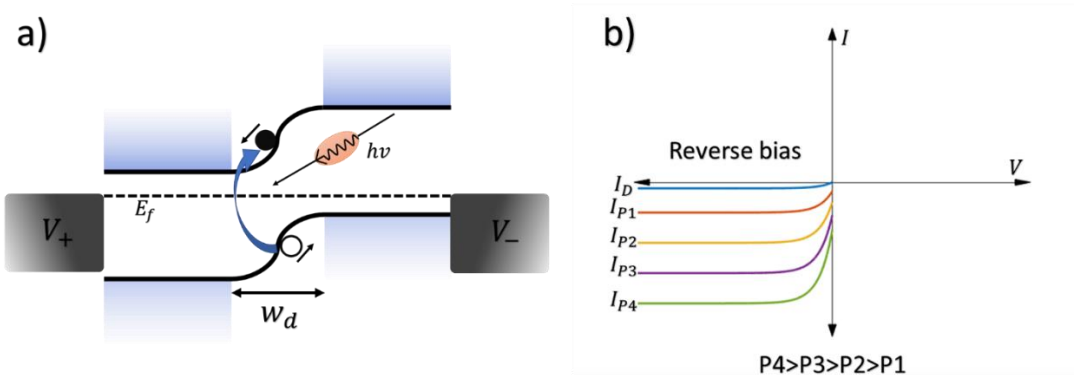

Figure 2.4.3 a) Band diagram of a photodiode in reverse bias under photoexcitation and b) I-V characteristics of a photodiode under dark condition and different optical excitation power levels.

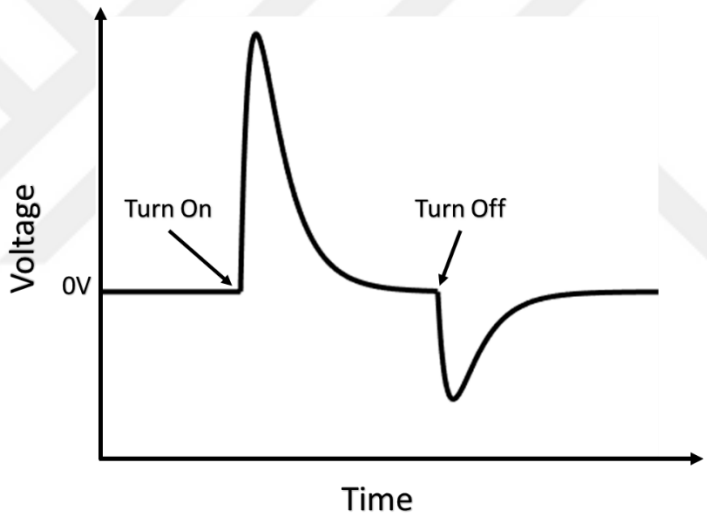

Figure 2.4.4 Voltage transient of a light sensitive nanocrystal skin (LS-NS).

Here we briefly explain the light-sensitive nanocrystal skins since this device platform is the photosensitive architecture on which we mainly focus in this thesis and has an unconventional working principle. Our group introduced LS-NS devices in 2010 in the previous report of S. Akhavan et. al. [13]. These capacitive devices utilize the photoinduced polarization of the metal-semiconductor contact, resulting in photovoltage build-up as the signal. Since two sides of such a device are insulated by an oxide layer, there is neither a current running through the device, nor there is a need for an external bias to be applied for the device to work. Therefore, these devices consume no power during operation [13]. Figure 2.4.4 shows a standard voltage-time

profile of the photovoltage build-up in the excitation phase and following dark conditions. Since there is no current running through the device, there needs to be a parallel shunt resistance connected to the device. The device is probed through both electrodes to read out the voltage across the device. Here the shunt resistance's main role is to control the rate of discharge of the photovoltage. The smaller the shunt resistance is, the faster the response is, however, the smaller the signal is too. This device has been operated under different conditions and a variety of device structures, including fragmentable and elastic substrates and tandem structures, have been previously reported through further iterations of the proposed device [19, 20, 21]. In all of these previous demonstrations of the LS-NS, however, the active absorbing material is the colloidal quantum dots. No LS-NS of CQWs has been shown to date.

Chapter 3

LIGHT-SENSITIVE MONOLAYER-THICK NANOCRYSTAL SKINS OF FACE-DOWN SELF-ORIENTED COLLOIDAL QUANTUM WELLS

This chapter is based on the article "Light-Sensitive Monolayer-Thick Nanocrystal Skins of Face-Down Self-Oriented Colloidal Quantum Wells", prepared by T. Bozkaya, F. Isik, I. Bozkaya, S. Delikanli, and H.V. Demir which is in submission [43].

Colloidal quantum wells, belonging to the quasi-two-dimensional sub-family of semiconductor nanocrystals, provide superior optical properties, as discussed earlier [22, 23, 24, 25, 26, 27, 28, 29]. CQWs possess a well-defined vertical thickness owing to their atomically-flat structure across the entire lateral extension [30, 31, 32, 33]. With a vertical thickness of few monolayers, such a quasi-two-dimensional quantum structure leads to giant oscillator strengths [34], giving rise to remarkably large absorption cross-sections. Their customizable absorption spectrum further provides another degree of freedom to tune their absorption-based photo-sensing functionality and performance in operation. Synthesized using wet chemistry, these CQWs are solution-processable to fabricate their devices, which significantly reduces their processing costs.

As introduced in the thesis recent research on CQWs has showed ways to self-assemble CQWs of a specific orientation [9, 10]. Since a self-assembly process can be employed to obtain only a single monolayer of CQWs in one targeted orientation in the film, such an orientation-controlling approach provides us with the ability to achieve excellent control also over the film thickness while keeping the film's roughness to a minimum to fabricate highly reproducible, precisely-constructed, high-performance devices [9]. As long as the sub-phase required for such a self-assembly method is chosen to be compatible with the substrate in use, this approach is essentially applicable to any substrate. It is also noteworthy to point out that the self-assembly process is carried out

under ambient conditions, which makes it cost-effective. Considering the capability to self-assemble a monolayer film of CQWs, combined with their favorable optical properties, CQWs offer great promise for absorptive devices such as photoconductors [35].

Based on optical absorption, light-sensitive nanocrystal skins are constructed in a non-conventional photosensitive device architecture that relies on the principle of photogenerated voltage build-up, demonstrated to be a versatile and efficient device platform [13]. The concept of LS-NS can be applied to different device architectures making use of tandem [21] and exciton funneling [19] configurations as well. Furthermore, this device structure has also been implemented on various substrates, including semi-transparent and flexible substrates [20]**,** [36, 37, 38]. Finally, since the photogenerated voltage build-up allows for a self-powered operation mode, this device platform does not require any external power supply, making it highly attractive from the external power consumption point of view [13].

In this thesis work, to utilize the attractive properties of CQWs and leverage on the orientation control in the self-assembly of CQW, we proposed and developed the LS-NS device platform of orientation controlled self-assembled 4.5 ML CdSe CQWs in the face-down orientation for the first time as the active layer, operating in the UV-visible range, as detailed in device preparation and characterization in the remaining of this chapter. Although a variety of LS-NS devices have been previously demonstrated using colloidal quantum dots [13, 19, 20, 21, 36, 37, 38], this is the first proof-of-concept demonstration of a LS-NS device based on the colloidal quantum wells [43]. This thesis work is also the first account of face-down orientation-controlled CQWs used in such an absorptive device.

3.1 Colloidal Quantum Well Preparation

CdSe colloidal quantum wells with the thickness of 4 monolayers were synthesized as given by a previously reported recipe in the literature [39, 40]. As the initial step, the reaction mixture in a three-neck flask, which consists of 340 mg of cadmium myristate, 24 mg of selenium, and 15 mL of octadecene (ODE) was vacuumed at 95°C for an hour and then heated to 240°C under Ar atmosphere. At roughly 195°C, 120 mg of cadmium

acetate dihydrate was quickly introduced to the reaction mixture when the color of the solution turned dark orange. For 8 min, the solution was stirred at 240°C, and with the addition of 1 mL of oleic acid, the reaction was cooled to room temperature in a cold-water bath. Further purification processes were used to isolate the 4 ML CdSe CQWs from other reaction products. The first step involved centrifuging the resultant mixture at 6,000 rpm for 6 min, separating the supernatant into another centrifuge tube. Second, ethanol was added to the supernatant solution until it turned turbid, and the precipitate was dissolved in hexane following the centrifugation at 6,000 rpm for 6 min. The absorption and photoluminescence spectra of the as-synthesized 4.5 ML CdSe CQWs in solution are presented in Figure 3.1.1a. Transmission electron microscopy of the as-synthesized CQWs are shown in Figure 3.1.1b, These CQWs provide an optical absorption cross-section of 9×10^{-14} cm^2 [12].

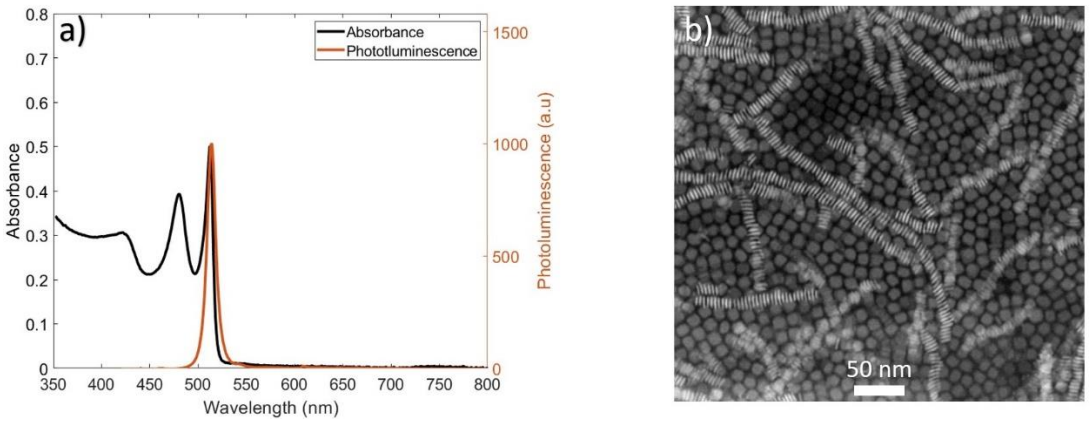

Figure 3.1.1 a) Absorption and photoluminescence spectra of the as-synthesized 4.5 ML CdSe colloidal quantum wells in solution. b) Their transmission electron microscopy image.

3.2 Colloidal Quantum Well Film Deposition and Device Fabrication

We conducted the self-assembly process of these CQWs as explained in a previous study [9]. Device fabrication using the CQWs was carried out according to a previous report [13]. Here we utilized Al_2O_3 instead of HfO_2 as the oxide layer as the current-blocking layer and shortened the processing time, different than the previous work. In the fabrication, we first coated ITO-precoated substrates having an ITO thickness of around 100 nm and sheet resistance of 2.5 ohm/sq with a 100 nm thick Al_2O_3 film at

300°C by atomic layer deposition (ALD). After this deposition, we proceeded with the self-assembly of CQWs on top of the dielectric layer. Finally, we coated a 40 nm thick Al on top of the CQW layer to make the final metal contact (Al) on the top by using thermal evaporation (see Figure 3.2.3d).

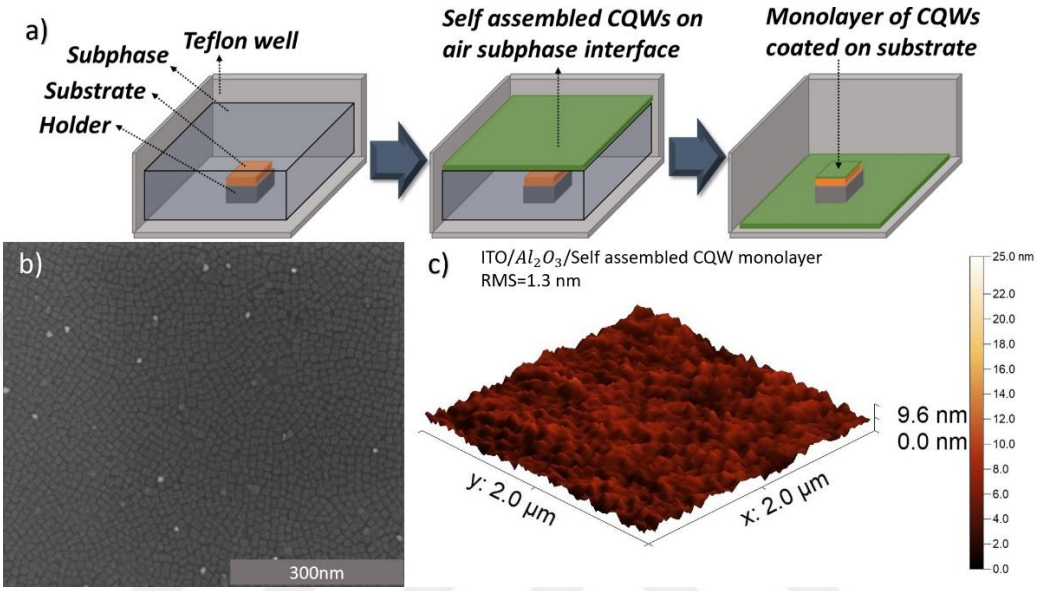

Figure 3.2.1 a) Process flow of the self-assembly process. b) Scanning electron microscopy (SEM) image of a monolayer face-down self-assembled 4ML CdSe CQW film c) Atomic force microscopy (AFM) of self-assembled 4.5 ML CdSe CQW film on top of ITO substrate coated with Al_2O_3 with thermal atomic layer deposition (ALD) method with film roughness of root mean square (RMS) 1.3 nm.

The self-assembly is a critical aspect of this study, considering the significant reduction of the surface roughness (see Figure 3.2.1c) and the robust control of the CQW film's thickness with its conformality of the layer (see Figure 3.2.1b). In the self-assembly process, we fixed the substrate on top of a holder using double-sided tape, placed it into a Teflon petri dish, and slowly poured the subphase inside the dish. Here it is critical not to leave any air bubbles inside the subphase, which can surface later and distort the self-assembled film at the subphase/air interface. Also, the subphase's height should be reasonable; if it is too low, the substrate and holder start to interfere with the surface interactions, and if it is too high, interactions increase with the edges of the well, making

it challenging to preserve conformality of the film during the draining process (see Figure 3.2.1a). Subsequently we carefully dropped the CQW solution on top of the subphase by using a micropipette at a predetermined amount. We waited until the end of the process of self-assembly while the solvent of CQWs evaporated slowly. After evaporation, with the help of an injector, we drained the entire subphase from the bottom of the container. Finally, we placed the substrate under vacuum until all remnants of the subphase evaporated completely. At the end of this step, we have the monolayer CQW film successfully placed on top of the substrate. The surface roughness of the CQWs was found to be 1.3 nm thanks to their successful self-assembly on top of the ITO/Al_2O_3 which also had reduce RMS surface roughness from 3.5 nm (for ITO substrate (see Figure 3.2.2a)) to 1.8nm (see Figure 3.2.2b).

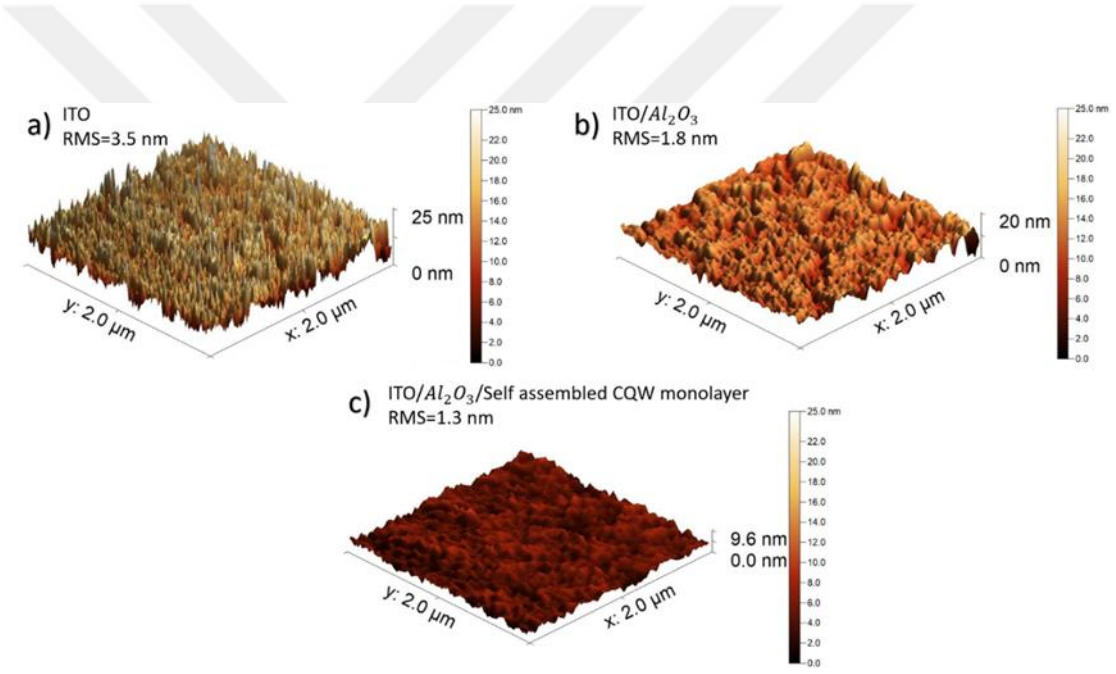

Figure 3.2.2 Atomic force microscopy of the device sample surface at different stages throughout the fabrication process to show the reduced RMS surface roughness: a) Commercial ITO substrate, b) alumina-coated ITO substrate and c) ITO/Al_2O_3/CQW structure.

To fabricate the LS-NS devices, we used commercially available 100 nm thick ITO-coated glass substrates from Osilla with dimensions of 7.5 cm × 2.5 cm (see Figure 3.2.3a). We cut each of the substrates into three even pieces of 2.5 cm × 2.5 cm and applied two subsequent cleaning procedures on each piece, one at a time, as follows: First, we cleaned the substrate pieces for 10 min in Hellmanex solution of deionized

water. Then, we washed them three times in deionized water for 5 min each. This is important to eliminate any residual contamination of the Hellmanex detergent. Afterward, we sonicated the pieces in acetone and isopropanol alcohol for 10 min each time. This completes the first cleaning, which removed most of the major residual contamination on the substrates. Next, we took the substrates to the cleanroom for delicate surface cleaning as the second step of cleaning process before the thermal ALD. In this second step, we also cleaned each piece separately. It is vital to use Teflon tweezers for this washing process. We cleaned the ITO surface of the substrate by first washing with a DI water fountain for around one minute and then washed the surface with acetone and isopropanol alcohol. Finally, we covered one of the edges for each substrate piece with Kapton tape (0.5 cm) to access the ITO contact when the tape was removed.

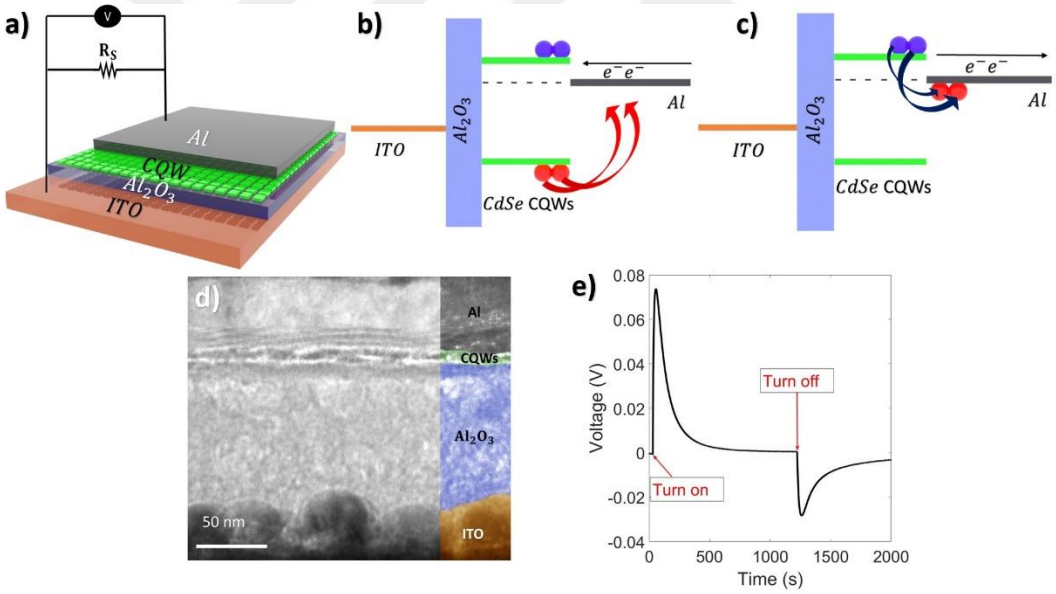

Figure 3.2.3 a) Illustrative schematic of the CQW LS-NS device, which shows each layer of the device, additionally depicting the external circuitry that consisting of contacts the external circuit, connected shunt resistance, and voltmeter, b) simplified energy band diagram showing the carrier transfer throughout the excitation phase of photovoltage build-up, c) simplified energy band diagram carrier transfer of the photovoltage build-up throughout the phase in which the excitation source is turned off, d) transmission electron microscopy image of the cross-section of the LS-NS device, e) voltage-time trace in standard device operation mode. Here the photovoltage build-up

is observed with "turn on" marking the point in time at which the excitation source is turned on. "Turn off" marks the point at which the excitation source is turned off.

Subsequently, we used ALD to coat a 50 nm thick Al_2O_3 film at 300°C (see Figure 3.2.3d). After letting the samples cool to room temperature, we took them out and washed them with DI water, acetone, and isopropanol alcohol again. The reason behind this additional cleaning procedure was to eliminate any possible tiny flakes that could possibly come from the ALD chamber during deposition. If such flakes are generated at an early phase of the deposition, they prohibit the growth of a uniform film, generating bare sites to possibly cause a short circuit across the device. After this washing step, we continued ALD to deposit the next oxide layer of 50 nm in thickness, and the oxide deposition process was completed with a total thickness of 100 nm of the deposited Al_2O_3 film. At this point, we moved on to the self-assembly procedure explained previously. Finally, we coated the aluminum contact on the top with thermal evaporation. One critical step to point out before the thermal evaporation is that we isolated each side of every substrate piece by 0.5 cm with Kapton tape. This was necessary to isolate the edges. Since edges are rough regions, it is possible to come across defects that might result in short circuits at the end. Finally, we ended up with an active area of 2.25 cm^2, since the dimensions of the active area in which we collected photogenerated charges is 1.5 cm × 1.5 cm.

3.3 Colloidal Quantum Well Device Operation and Characterization

To measure voltage, we used Keysight B1500A semiconductor parameter analyzer probe station, where samples were placed on top of a glass stand and contacts were made by utilizing its probes at both ITO and aluminum sides. A 405-nm emitting LED was connected to an external power source for the excitation. Also, we used a custom-made monochromator in the same setup to further obtain the spectral sensitivity by changing the LED excitation source with this monochromator when needed. To assess the optical excitation power, we used an optical powermeter for both cases before inserting the LS-NS device into the setup. The probes connected to the device itself

were also connected to a shunt resistor in parallel so that the device discharge could also take place at a controlled rate.

Owing to the device architecture of this LS-NS platform (see Figure 3.2.3b), carriers cannot pass through the device because of the current-blocking dielectric film of Al_2O_3. Hence, when not connected, the device is in open circuit and acts like a parallel-plate capacitor to be charged upon optical excitation, starting from uncharged state. Under optical illumination, electron and hole pairs are photogenerated in the self-assembled monolayer of CQWs and dissociated at the CQW-Al interface. Holes are then transferred to and accumulated in the Al side, whereas electrons stay on the CQW side due to the work function of Al and the valence and conduction bands of the CQW layer. Therefore, in the LS-NS device, positive and negative charge accumulations are internally on the opposite sides (in the Al and CQW layers, respectively), as sketched in Figure 3.2.3b. Those dissociated electron-hole pairs at the CQW-Al interface are held across the device capacitively as the stored charges.

The photovoltage build-up highly depends on the capacitive polarization of the metal-semiconductor contact as the device itself is in a transient state. This LS-NS device can be considered as an RC circuit element. When connected externally through a shunt resistor of a predetermined value, the LS-NS device is able to discharge the photovoltage at a desired rate (see Figure 3.2.3a). As can be seen in Figure 3.2.3b, externally circulating electrons neutralize the polarized device. As a result, one observes a transient voltage response (voltage vs. time) as presented in Figure 3.2.3e (during the excitation phase), which grows exponentially due to the continuous excitation and simultaneously, continuously decays due to the RC decay. After the excitation source is turned off, the photogenerated electron-hole pairs are no longer separated; instead, electrons on the CQW side start recombining on the aluminum side, as illustrated in Figure 3.2.3c. This situation leaves externally neutralizing electrons as additional charges on the aluminum side (leaving behind holes alone as the positive charges on the ITO side). This leads to an inverse voltage build-up (see Figure 3.2.3e) with a magnitude correlated to the time and intensity of optical illumination, which can be interpreted as a memory effect [13].

$$\mathbf{V(t) = A\left(1 - e^{-G(t-t_0)}\right) \times e^{-\frac{1}{R_S C}(t-t_0)}} \qquad \text{Eq. 3.3.1}$$

We use Eq. **3.3.1** to express the photovoltage build-up as a function of the time. Here, the term A represents the upper capped value of the build-up voltage, which purely depends on the number of photogenerated excitons available for separation. The first term of Eq. **3.3.1** is an inverse exponential process in time. The second term on the right-hand side of Eq. **3.3.1** is the RC decay term of a parallel plate capacitor. This represents the discharging process of the device via the external circuitry through the parallel shunt resistor connected to the device. These first and second terms of Eq. **3.3.1** are multiplied because they are simultaneous processes competing with each other. In Eq. **3.3.1**, R_S denotes the resistance of the externally connected shunt resistor. C stands for the effective capacitance of the device between the ITO and aluminum contacts. Finally, G stands for the generation rate. Here note that G and A are both empirically measured.

Next, we investigated the relation of the excitation power to the device operation by systematically varying it. We observed here with the self-assembled CQW monolayer as the device's active film that the RC decay mechanism is profoundly affected in the LS-NS devices (see Figure 3.3.1). We found that the RC decay time constant of the device is decreasing as we repeat the turn-on and turn-off cycles consecutively. This decrease can be attributed to the change in effective device capacitance and it is considered to be a consequence of the change in the effective dielectric constant of the CQW layer [41]. The overall capacitance is decreased throughout the device for consecutive measurements (repetition numbers 2, 3 and 4). As the excitation power changes, we observed a slight variation in the RC decay time, a critical parameter for calculating the capacitance and effective dielectric constant. Here we obtain a significantly larger capacitance for CQW LS-NS devices around 55 nF for each power setting, whereas for colloidal quantum dot (CQD) based LS-NS devices this value is averaged at around 38 nF for each power setting. More significantly, if we look at the values of capacitance per unit area, we find 24.44 nF/cm^2 for CQW LS-NS (2.25 cm^2 of active area) and 0.79 nF/cm^2 for CQD LS-NS (48 cm^2 of active area) [13]**.**

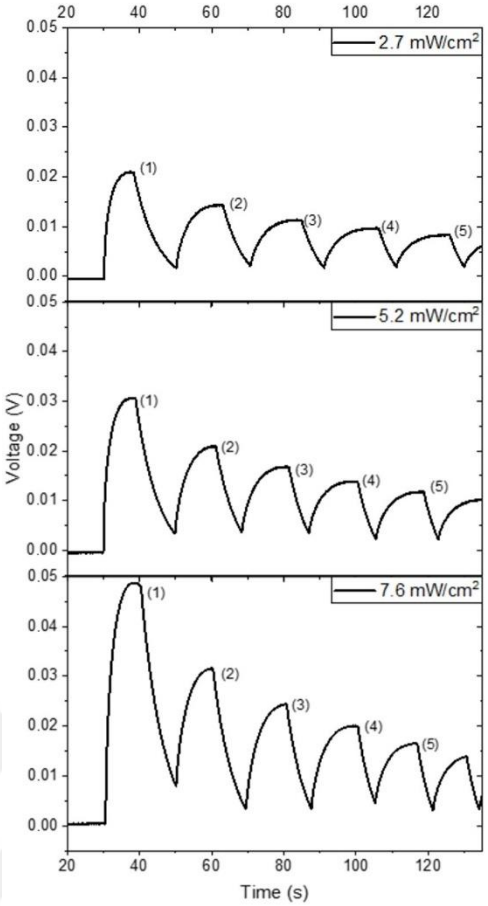

Figure 3.3.1 Photovoltage build-up and RC decay of LS-NS device, upon turning on and off the excitation source (for 5 times as displayed) at different excitation power levels at 405 nm: 2.7, 5.2 and 7.6 mW/cm^2.

Table 3.2.1 RC decay times calculated at the turn off points in Figure 3.2.5 at the corresponding excitation power level.

	2.7 mW/cm^2			**5.2 mW/cm^2**			**7.6 mW/cm^2**		
	RC (s)	**C (nF)**	ε_{CdSe}	**RC (s)**	**C (nF)**	ε_{CdSe}	**RC (s)**	**C (nF)**	ε_{CdSe}
1	5.42	54.2	0.26	5.51	55.1	0.28	5.48	54.8	0.27
2	4.57	45.7	0.23	4.54	45.4	0.23	4.58	45.8	0.23
3	3.97	39.7	0.20	3.91	39.1	0.20	3.92	39.2	0.20
4	3.46	34.6	0.18	3.31	33.1	0.17	3.47	34.7	0.18
5	3.07	30.7	0.16	3.00	30.0	0.15	3.08	30.8	0.16

Also, we studied the excitation power dependence of the photovoltage build-up (see Figure 3.3.2a). As the excitation power increases, we observe a decrease in the sensitivity (see Figure 3.3.2b) due to the saturation of the active layer. Furthermore, we conducted spectral sensitivity measurements to understand the spectral response of the CQW LS-NS device. For this characterization, using a monochromator, we scanned the optical excitation spectrum from 450 to 550 nm. We recorded incident optical power while carrying out the photovoltage build-up measurements at each wavelength. Next, we calculated the peak sensitivity for each measurement (see Figure 3.3.2c). On the measured spectral sensitivity curve, we observe the first (heavy-hole) and second excitonic (light-hole) absorption peaks of the CQWs as this curve mimics the spectral profile of the optical absorbance of CQWs. This similarity provides another opportunity for the device to utilize; with the right design and filtering, one can simultaneously utilize the same active material (CQWs) as an active layer in different multiple spectrum windows. Finally, we observe a cut-off wavelength near 512 nm for these CQWs. Similarly, we do not read any signal from our device beyond this spectral point. Thus, the measured sensitivity is practically zero above the cut-off wavelength of 512 nm.

Another critical aspect is that optical absorption levels out in the spectral range shorter than the 375 nm on the absorbance spectrum, while what we observe in the sensitivity spectrum is quite the opposite since the spectral sensitivity keeps growing. Because each absorbed photon with higher energy than the cut-off value creates an electron-hole pair independent of their energy. However, excess energy is also transferred into the photogenerated pair; conventionally, this energy is thermally lost as the electron and hole relax towards the band edge. However, in the device's operation, we utilize the hopping of the charges across the aluminum interface and the CQW layer, for which excess energy becomes helpful. Effective separation occurs at the interface, and effective separation at the contact leads to a larger voltage build-up, hence the increased sensitivity.

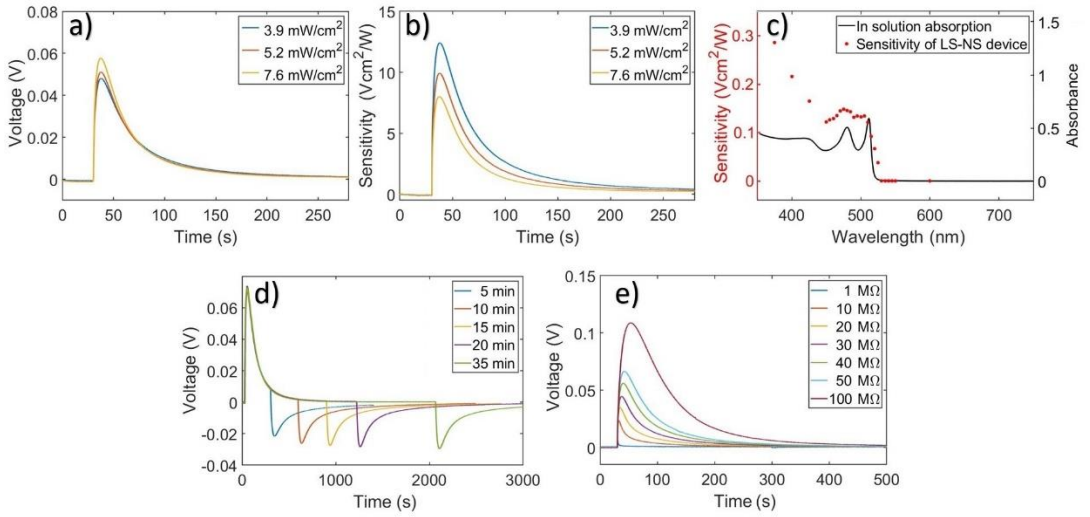

Figure 3.3.2 a) Photovoltage build-up at different excitation power levels at 405 nm. b) Photosensitivity calculated by dividing the photovoltage build-up curve by the excitation power. c) Spectral photosensitivity plotted together with spectral absorbance. d) Photocharging effect shown through photovoltage build-up measurements by turning the excitation source off at different time marks at the same excitation power at 405 nm. e) Photovoltage build-up utilizing 405 nm excitation source at the same power using parallel shunt resistors connected with varied resistance.

Furthermore, we studied the photocharging effect. We found out that, as the time of illumination increases, we observe a larger negative peak once the excitation source is turned off (see Figure 3.3.2d), (when we use a constant excitation power level during the excitation time). This effect is directly proportional to the total number of collected electrons from the external circuitry during the excitation phase. This phenomenon is explained as a memory effect [13]. If we compare our CQW LS-NS device with its CQD counterpart in terms of the photocharging capability, we can see that CQW-based devices has a larger photocharging capability. The CQD LS-NS reaches a maximum negative peak of 20 mV after 30 min of illumination, however our CQW LS-NS reaches the similar negative peak of 20 mV only after 5 min of illumination and later a maximum of 30 mV after 35 min of illumination [13].

Our final characterization was the photovoltage build-up of the CQW LS-NS device with different values of shunt resistance (see Figure 3.3.2e). The signal amplitude grows as the shunt resistance increases. This trend of increasing voltage complies with the predictions of Eq. **3.3.1**. Since the generation parameter is constant (the first term of Eq. **3.3.1**), the RC time constant that is growing larger with increasing the shunt resistance exposes the device to a slower decay. As a result, we obtain an increasing trend in the photovoltage build-up despite a slower response.

3.4 Summary

In this thesis work, we demonstrated and systematically characterized our LS-NS device fabricated using face-down oriented CQW monolayer for the first time. We investigated photocharging effect, spectral sensitivity, and decay times. We observed that, as the excitation power is increased, the peak photovoltage build-up increases while the sensitivity decreases $(V \times cm^2)/W$. Moreover, the spectral sensitivity profile of the LS-NS device complies with the first and second excitonic peaks of the absorption of the CQWs. We also found that the photocharging effect is apparent as the excitation is turned off. Finally, as external circuitry is made increasingly more resistive, the photovoltage build-up curve grows in amplitude because of the strongly capacitive behavior of the device at the cost of a slower device response. These findings indicate that face-down CQW-based LS-NS devices hold great promise for photosensing applications.

Chapter 4

SENSITIVITY ENHANCEMENT BY IMPROVEMENT OF CHARGE TRANSFER IN NANOCRYSTAL SKINS OF ORIENTATION CONTROLLED COLLOIDAL QUANTUM WELLS

The edge-up orienting self-assembly process is applied to our colloidal quantum wells to allow to study different interfaces of the quasi-two-dimensional structure [9, 16]. Considering their 4.5 monolayer structure, both faces are dense with cadmium atoms, which include the oleic acid ligand binding centers and provide finer passivation at the faces [42]. However, since those ligands are long and not conducive, they prohibit the charge hopping mechanism, reducing the conduction at the faces. However, selenium atoms are more likely to be present on the edges. In addition, cadmium vacancies are denser at the edges and provide defect centers that are not passivated with the oleic acid ligands, which reduces the insulation of the CQWs at the edges and makes the process of charge hopping at the edges possibly easier. Hence, we expect electrically anisotropic behavior of the CdSe CQWs in the edge-up orientation considering charge hopping and conduction behaviors.

4.1 Colloidal Quantum Well Film deposition and Comparison

We fabricated two identical LS-NS devices except for the edge-up orientation-controlled and randomly oriented active layers. In these LS-NS devices, we employed either edge-up oriented self-assembled CQWs or the randomly oriented spin-coated CQW as the active layer. 4.5 ML thick CdSe CQWs were used and they were synthesized according to the recipe given in the previous chapter. The schematic of the

LS-NS device having edge-up oriented self-assembled CQWs as the active layer is given in Figure 4.1.1a. To fabricate the LS-NS device, we first deposited 50 nm thick Al_2O_3 layer as the current-blocking oxide layer using atomic layer deposition on a precleaned ITO-coated substrate. Then, the active CQW layer was deposited using either the spin-coating or the self-assembly method. It is worth noting that the absorbance of the spin-coated layer matched the absorbance of the single layer of the edge-up oriented CQW layer by adjusting the concentration of the solution used in the spin-coating. Details of the deposition of the edge-up oriented CQW layer and the spin-coated CQW layer are provided in the following sections. Finally, we deposited 40 nm thick Al using thermal evaporation similar to the previous chapter.

The self-assembly process we utilized for the edge-up oriented film slightly differs from the face-down oriented film process discussed in the previous chapter. For the edge-up oriented self-assembly to take place, we need stronger differentiation of the polarity between the subphase and the solvent of the CQWs compared to that of the face-down orienting self-assembly process [9]. Initially, by adding ethanol, we precipitated the CQWs, which were dispersed in the hexane solution. Then, we dispersed the precipitated CQWs in octane, which is less volatile than hexane. The slower evaporation of the octane helps the self-assembly process once the CQW solution dropped on top of the subphase. For the edge-up self-assembly we employed ethylene glycol as the subphase of choice. Except the choice of solvent, the subphase self-assembly process is similar to the previously described technique.

Even though it might seem straightforward, some critical points need to be explained for the spin-coating process. The role of the spin-coated film in this work is to make a fair reference in order to compare the electrical characteristics at the contact boundary of the random oriented (spin-coated) and the edge-up oriented films. So, to achieve a fair comparison, we also washed the CQWs dispersed in hexane one more time since every washing process clears the CQW solution from the free ligands (which are excess organic ligand chains available in the solution and not bound to surfaces of the CQWs). To do that, we precipitated the CQW solution with the addition of ethanol into the solution. We dispersed the precipitation again with the same amount of fresh hexane, similar to the previous step but hexane this time. Before we moved on with the actual spin-coating processes to set the spin-coating parameters right, we first measured the spectral absorbance of the edge-up coated film. Afterward, by spin-coating the dummy

samples, we matched the on-film absorption of the edge-up oriented film with the spin-coated film. With the first dummy sample, we measured the spectral absorbance for the spin-coated film. We then diluted the spin-coating solution with additional hexane to reduce the film absorption for the next iteration until we matched the spectral absorbance of the edge-up coated film. All the spin-coating processes were carried out at 2500 RPM with a 50 μL of CQW solution dropped and spun for 30 s. One can increase the amount of solution dropped for spin-coating for larger surface-area films.

For the edge-up oriented film, we observe that the film was brought together by the collection of the edge-up oriented much smaller groups of stacks that were oriented in different directions, as can be seen clearly in Figure 4.1.1b. Even though these smaller stacks are made of 5-10 CQWs or 30-40 CQWs for the larger stacks, there is a variation in the sizes of the stacks. However, on the larger scale, the surface coverage of CQWs is excellent. There is a chance that one might spot a mild amount of face-down oriented CQWs in the edge-up film. However, this face-down oriented CQWs in the film are a pretty small minority of the film, and since the self-assembly process is a statistical process in which it is pretty possible few of the unit particles could be stuck at the larger energy regimes (face-down oriented CQWs). However, it is fair to say that those face-down oriented CQWs in the edge-up superstructure make a significantly small minority. On the other hand, edge-up oriented stacks make up a large majority of the film; hence we can consider the film mainly in the orientation of edge-up (see Figure 4.1.1b).

On the other hand, the opposite is true for almost all of the parameters for the spin-coated film. For this specific film, we observe that CQWs were gathered in clusters in a "web-like" structure, and they do not consist of a monolayer structure in those cluster regimes but thicker regions. This cluster formation leads to a nonconformal film that lacks surface coverage. At the same time, when we look closer at those clusters, we realize that CQWs are randomly oriented between the orientations of edge-up and face-down; however, the amount of the edge-up oriented CQWs is significantly low (see Figure 4.1.1c).

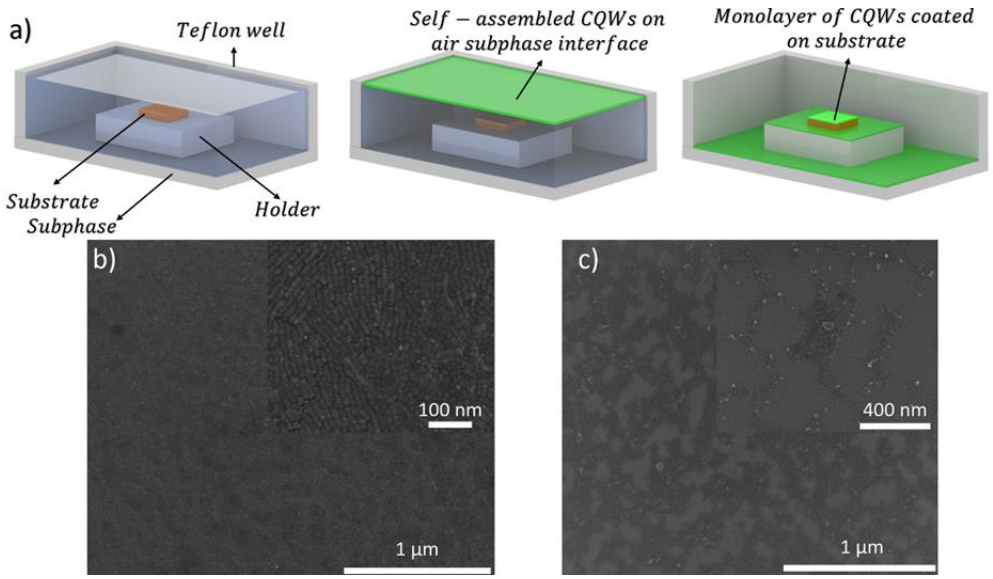

Figure 4.1.1 a) Process flow schematic of the self-assembly process. b) Scanning electron microscopy (SEM) image of monolayer edge-up self-assembled 4.5 ML CdSe CQW film. c) Scanning electron microscopy image of the spin-coated film of 4.5 ML CdSe CQWs of which optical absorption is matched (to that of the edge-up film).

The most important figure of merit to compose a fair comparison between both devices is the absorbance values of the active layers for the edge-up and spin-coated films. Since we are working in a regime of single-layer films for the case of self-assembly, which has a thickness near 20 nm depending on the dimensions of the CQWs, it is pretty hard to achieve the same thickness all around the film considering the nature of the spin-coating with nanoparticles. Instead, the film's absorption is a more reliable reference point for characterizing the two devices. The exact amount of absorption on two films means the same number of photons are absorbed. Since both films are made of the same material, and the only difference between them is the orientation of the CQWs, one would expect a similar amount of excitons to be generated. Moreover, after that generated signal would inform us more accurately about the differences at the metal-semiconductor boundary stemming from the difference between the orientation of the CQWs.

4.2 Characterizations and Comparison of LS-NS Devices with Edge-Up and Spin-Coated CQW Active Layers

We performed electrical and optical characterizations on the device to characterize, compare, and highlight the significant differences between the self-assembled and spin-coated films. First, one needs to pinpoint that the LS-NS devices work on the principle of photovoltage build-up (see Figure 4.2.1a). Since this is a dynamic process that is highly affected by the charge transport rates as it was described with the rate of generation and the rate of decay terms in Eq. 3.3.1. The orientation of the CQWs (being in random orientation (see Figure 4.1.1c) or stacked edge-up (see Figure 4.2.1b) (see Figure 4.1.1b)) significantly impacts the rate of charge transport during the phase of "turn on" (see Figure 4.2.1c) and "turn off" (see Figure 4.2.1d) , considering the anisotropic nature of the CQWs in terms of shape and ligand distribution along the edges and the faces resulting from the quasi-2D structure.

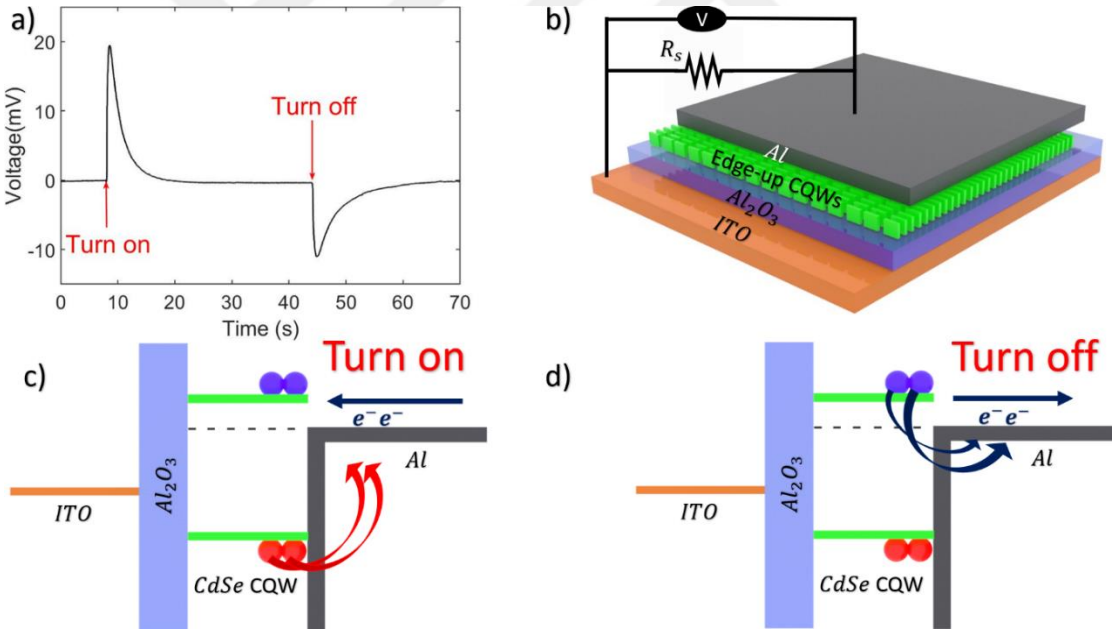

Figure 4.2.1 a) Standard device operation mode; here, the photovoltage build-up through time is demonstrated. The "turn on" is the point of time that the excitation source is turned on, and the "turn off" time marks the point of time that the excitation source is turned off. b) Illustrative schematics of the LS-NS device of edge-up oriented CQWs. c) Simplified scheme of carrier transfer throughout the excitation phase of the photovoltage build-up. d) Simplified scheme of carrier transfer of photovoltage build-up during the phase in which the excitation source is turned off.

Both films exhibited a similar amount of absorption (Spin-coated film has a slightly larger absorption). However, we can see that edge-up oriented film performs up to five-fold of the spin-coated active layer in terms of peak voltage signal when we observe the repetitive photovoltage build-up measurements (see Figure 4.2.2b). At the same time, we need to underline that both devices mimic the behavior of the absorption curves on the spectral sensitivity curves while edge-up being much more sensitive (see Figure 4.2.2c). However, similar to the previous chapter, towards shorter wavelengths, we see that the sensitivity rises above the first and second excitonic peaks in magnitude. We observe the opposite for the spectral absorption curves since the absorption levels out and keeps at a lower level than the excitonic peaks below 425 nm. We discussed this phenomenon briefly in the previous chapter; however, this phenomenon leads us to an essential mechanism behind improving charge transfer. We reckon that excess photon energy is utilized during the charge hopping process, which contributes to a faster rate of charge transfer.

So, the transfer of charges happens between the metal and semiconductor interface; however, during this transfer process, we utilize the charge hopping mechanism, which can be considered as a finite barrier problem. Two possibilities are apparent at this point: tunneling the charges through the finite barrier or thermal hopping of the charges across the barrier. We relate this rise in the spectral sensitivity to the excess energy transferred to the excited exciton pair. Under normal circumstances, this excess energy would excite the electron and hole to higher energy levels, and that energy would be thermally lost; however, at the interface of metal-semiconductor, we utilize the hopping of the charges, and this excess energy provides an upper hand for the charge hopping process. Holes with the extra energy are transferred across the metal-semiconductor contact at a higher rate. Because of this improved charge transfer, we observe an increase in the spectral sensitivity to the left of the graph (for shorter wavelengths and hence the larger energy per pair) even though we have less absorption in that spectral region (see Figure 4.2.2c).

In Figure 4.2.2a, we observe that 4.5 monolayer CQWs consist of cadmium and selenium atoms in their crystal structure. We can see that the faces of the CQWs are dense with cadmium atoms. Those atoms are the spots that oleic acid ligands are attached to provide colloidal stability and passivation of the nanocrystals. Even though this passivation is necessary to keep the crystal intact and unreactive, not to deteriorate, it is less desirable electrically since oleic acid ligands are long and not conductive. They provide a potential barrier between the semiconductor crystal and the metal contact. However, if we look more closely, we can see that at the edges of the CdSe CQWs, selenium atoms stick out from the crystal structure. In addition, cadmium vacancies can be considered bare sites since ligands do not attach to them, and we think at the contact of the metal those sites provide lower energy and shorter barriers for charges to hop across. Then edges of the CQWs would provide low energy shorter width potential barriers for the charge hopping and would improve the charge transfer rate in that direction, hence improving the device sensitivity since the exciton pairs are dissociated at the metal-semiconductor interface more effectively. The improvement of charge transfer explains the sensitivity enhancement for both of the cases. In spectral terms, towards shorter wavelengths, we increase the energy of the exciton pair, which is utilized in the hopping process. However, for the orientation-controlled case, we improve the charge transfer by manipulating the finite barrier dimensions; hence, we improve the charge transfer and sensitivity. This is why edge-up-oriented CQWs perform better than randomly-oriented CQWs.

Apart from the sensitivity measurements, we conducted repetitive voltage-time measurements. In this measurement, we started the excitation phase and waited until the device returned the neutral state under excitation. Once the devices were neutral, we turned off the excitation source and waited until the negative voltage was dissipated. Once the device was entirely neutral, we turned on the excitation source again, completing one cycle. We conducted four of those cycles consecutively (see Figure 4.2.2b) to show the device's repetitive operability and compare the signal amplitudes and response times. We undertook both measurements (spin-coated and edge-up) under a constant optical power at 16.1 mW/cm^2 at 405 nm. Before comparing the devices, we observe that the first cycle of each device has a slightly larger peak than the following three, and the following three peaks are at the same amplitude. This is because the long-living trap states do not return to their steady states before the next cycle starts and do

not contribute to voltage build-up for the consecutive runs. However, they excite and contribute to the first cycle, so the first cycle has a slightly larger peak than the following ones. This behavior is shared between the edge-up and the spin-coated device.

Another aspect to point out for charge transport enhancement is the decay rates. We can observe that, even though the spin-coated film has a smaller signal amplitude, it decays to a neutral state slower than the edge-up devices. We can see that the voltage-time curve of the excitation phase of the spin-coated device crosses the voltage-time curve of the edge-up oriented device and decays more slowly to a neutral state. Furthermore, we find that the edge-up device has a four-fold larger signal amplitude than the spin-coated (see Figure 4.2.2b). This phenomenon is again caused by the faster rate of charge transport across the edge-up-oriented device.

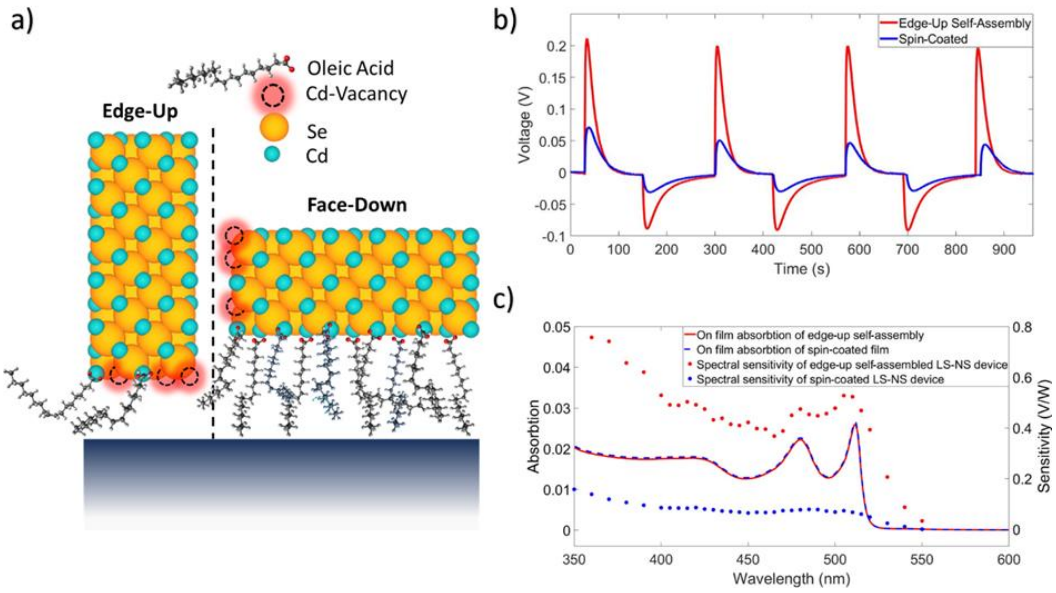

Figure 4.2.2 a) Illustrative schematics of CQWs in contact with the Al. Underlining crystal structure along with ligand distribution along the faces and edges with Cd vacancy sites. b) Consecutive photovoltage build-up operation of CQWs. C) Spectral sensitivities of both the spin-coated and self-assembled devices, along with the corresponding spectral absorption spectra.

Another important study we conducted was the power-dependent voltage time graphs of both devices. Here we fabricated identical devices, as was underlined before, with the same surface area and the same level of film absorption. However, only the orientation of the active films is different; one is edge-up oriented, and the other one is spin-coated. We have conducted excitation power-dependent voltage build-up measurements of those devices under different excitation powers. Here additionally, we measured the peak sensitivities for each voltage-time measurement. We can see that signal amplitude also increases for both devices in Figure 4.2.3a. However, one needs to underscore that, as the excitation power increases, the sensitivity of the devices starts to fall drastically, which is apparent for each device (see Figure 4.2.3b). More significantly, we observe that differentiation between signal amplitudes of the devices starts to lower as the excitation power increases. To analyze this phenomenon, we also calculated the ratio of peak sensitivities (spin-coated / edge-up) depending on the excitation power, and find see that this ratio starts to converge to the unity for sufficiently high excitation powers. The reason behind this is that the photovoltage build-up principle is a voltage signal capped to a value because of the open circuit structure of the device, and this is directly proportional to the number of available excitons to dissociate at the semiconductor-metal contact. So, even though at low powers, we find that the edge-up device outperforms the spin-coated one because of the easier dissociation of electron-hole pairs at the interface relatively to the spin-coated. At large enough excitation powers, we observe that the sensitivity of each device converges to an equal level because our initial constraint on the devices is that both active films have the same absorption and are safe to assume the same amount of exciton pairs generated to separate. However, the edge-up film can achieve that faster than the spin-coated one. Therefore, for immense enough excitation powers, ideally, we expect both voltage-time curves to converge to the saturation value since at those powers for both devices the generation rate is much larger than the RC decay rate. We observe that phenomenon happening in Figure 4.2.3b.

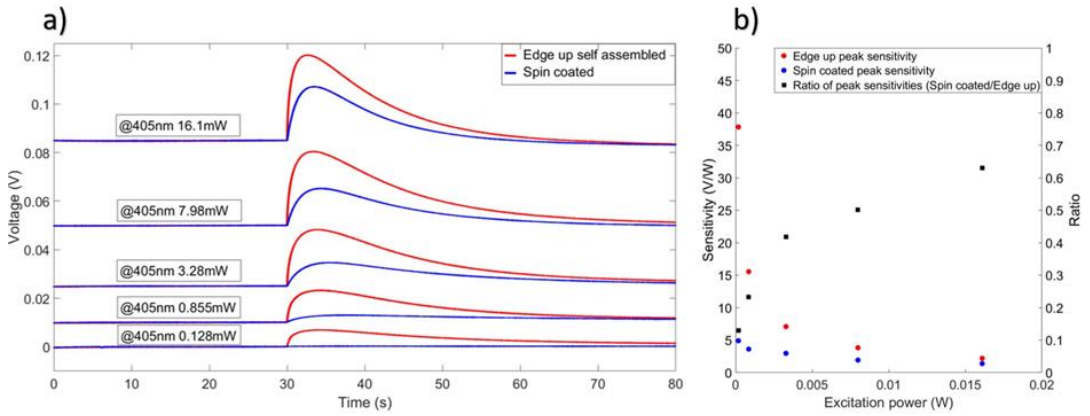

Figure 4.2.3 a) Excitation phase of photovoltage build-up curves under different excitation power levels drawn on the same scale. b) Excitation power-dependent sensitivity graph calculated through the peak signal of corresponding photovoltage build-up along with the ratio of sensitivities (spin-coated/edge up).

Another measurement that we conducted was the consecutive decay time measurements on the devices to differentiate and understand how the orientation of the active layer affects the decay times of the devices. This measurement was carried out previously on the face-down oriented devices to understand the effects of consecutive decays on the device. On the other hand, we conducted power-dependent decay measurements. We could not detect any significant difference in power-dependent measurements other than the peak signal amplitude; however, as the measurements take place consecutively, we detected that the RC decay time decreases as the measurements continue. The change in the effective dielectric constant of the device across the contacts is considered to cause this observation. However, in this work, we compare the differences between the edge-up and the spin-coated device's decay times, and what we observe here in Figure 4.2.4 is that the edge-up device yields a more prominent signal peak.

Similarly, we observe a quicker response for both the rise-up and decay. In Table 4.2.1, we observe that there is more than three-fold faster decay time for the edge-up device, which points out that there is a significant difference between both layers considering the charge transfer across the metal-semiconductor contact. In addition to the previously mentioned properties caused by the edge-up and face-down orientation differences of the CQWs, there is a significant difference between the surface topologies of the deposited CQW films considering one of them is a smooth and conformal film. And for the spin-coated one, there is a clustering in the spin-coated film. The primary source of the surface roughness is also causing the differentiation of the capacitance of the contact.

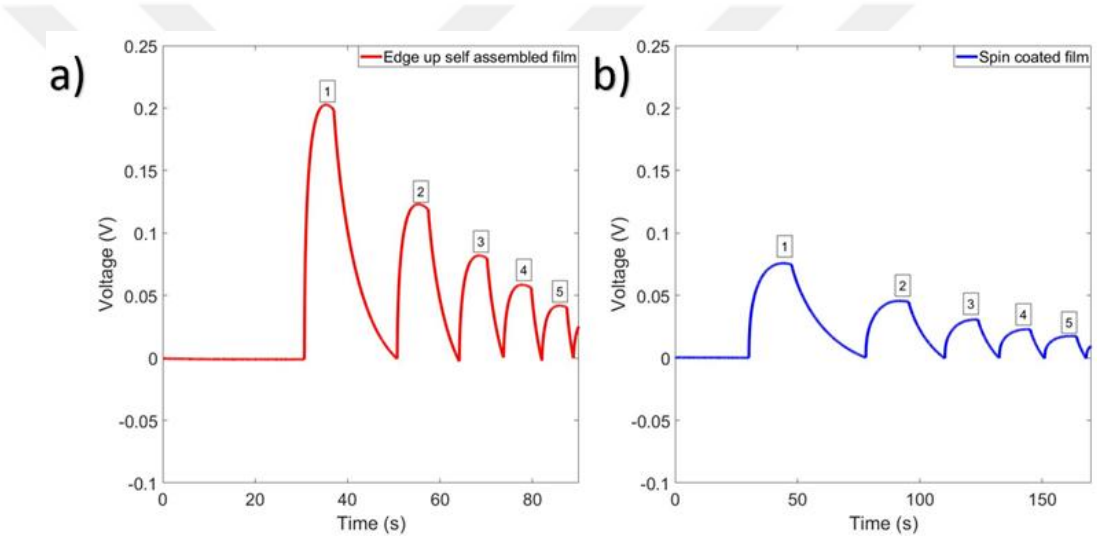

Figure 4.2.4 a) Repetitive decay curves of the edge-up oriented self-assembled film device by the method of consecutive excitation turning of the source. b) Repetitive decay curves of the spin-coated film device by the method of consecutive excitation turning of the source.

Table 4.2.1 RC decay times of each marked decay for both the spin-coated device and edge-up self-assembled devices. Accordingly, capacitances and effective dielectric constants are also determined.

Position in figure #	**Edge-up Self-assembled Device**			**Spin-coated Device**		
	RC (s)	C (nF)	ε_{CdSe}	RC (s)	C (nF)	ε_{CdSe}
1	4.56	45.6	0.22	15.5	155	0.74
2	2.72	27.2	0.13	6.47	64.7	0.31
3	1.72	17.2	0.08	4.16	41.6	0.20
4	1.12	11.2	0.05	3.08	30.8	0.15
5	0.76	7.6	0.03	2.02	20.2	0.09

4.3 Summary

In this thesis work, we developed and demonstrated the LS-NS device platform, which operates in the UV-visible range by utilizing the edge-up oriented self-assembled 4.5 ML CdSe CQWs for the first time as the active layer of the device. Here we compared the performance of the edge-up oriented self-assembled CQWs with the randomly oriented spin-coated CQWs in the LS-NS device. To make a fair comparison between both devices, we adjusted the spin-coated film's parameters until the absorption of the spin-coated film matched the absorption of the self-assembled film. In doing so, we ensured both films had the same optical absorption before fabricating the devices for a fair comparison. The first property between both films (edge-up and randomly-oriented

spin-coated films), we investigated was the SEM analysis to visualize differences between both films. We found that CQWs were in a stacked orientation in a conformal film of monolayer CQWs. The spin-coated film had a web-like structure of randomly-oriented CQWs clustered together in some spots but left bare spots on the nonconformal film. We investigated the performance of the fabricated devices through spectral sensitivity measurements, repetitive photovoltage build-up curves, excitation power-dependent photovoltage build-up curves and excitation power-dependent sensitivities, and decay curves. We first realized that the edge-up oriented device significantly outperformed the spin-coated device with up to nearly 8-fold peak signal enhancement. Considering that both films have similar absorptions, much of the performance enhancement cannot be attributed only to the enhancement of the film conformality and roughness. So, we are convinced that there must be a property that is affected by the orientation of CQWs. Cadmium sites on the edges pose vacancy-type defect sites, which lack passivation. Those vacancy-type defect sites are more densely localized at the edges rather than the faces [42]. Here we reckon that they improve the charge transfer by charge hopping between interfaces like CQW-aluminum and result in a faster charge transfer property, which results in the enhancement of the photovoltage build-up, hence the enhancement of the LS-NS device performance.

Chapter 5

Conclusion and Outlook

In this thesis, we have developed and demonstrated an LS-NS device employing the face-down, edge-up, and randomly (spin-coated) oriented self-assembled monolayer of all solution-processed CQWs as the active layer of the device platform. We reduced the surface roughness of the CQWs to 1.3 nm via their face-down oriented self-assembly. These devices are highly efficient in terms of power consumption since they work on the principle of photogenerated voltage build-up. This operation principle requires neither external biasing nor externally applied current running through the device.

In the thesis we found that spectral sensitivity mimics the absorption spectra of CQWs at the excitonic peaks as expected. However, at the lower end of the spectrum, we found a sharp rise of sensitivity different from the absorption spectra of CQWs. This difference is attributed to the more effective separation of excitons at the CQW-Al interface due to the excess energy provided by the higher-energy photons. The effect of shunt resistance is vital to a balanced operation; as its value increases, the voltage build-up increases at the cost of a slower response, which also complies with the mathematical predictions we made.

Also, in the thesis we have demonstrated and compared the edge-up oriented self-assembled active layer light sensitive nanocrystal skin device of CdSe CQWs with its counterpart spin-coated active layer light sensitive nanocrystal skin device. Here most significant result was the amount of improvement of the signal output of the device just by orienting the colloidal quantum well nanoparticles of CdSe in the edge-up direction for a vertical device structure while keeping the total absorption of both spin-coated and edge-up oriented equal. We obtained up to 8-fold signal amplitude enhancement for the edge-up oriented device relative to its spin-coated counterpart. We have also concluded this improvement is mainly dependent on the denser amount of cadmium vacancies that are collected at the edges relative to faces. Considering those vacancies enhancing the charge transport mechanism for the charge hopping.

In the light of our recent studies of the light-sensitive nanocrystal skins of orientation controlled colloidal quantum wells alongside the proposed mathematical expression of the photovoltage build-up principle, LS-NS devices enables us to investigate further aspects of the both field of photosensitive devices, and ability of meticulous research of metal-semiconductor contact interface.

First, in light of the recent proven ability to utilize orientation-controlled techniques of self-assembly, one can further study the different active layer settings such as multilayer self-assembled active layer of colloidal quantum wells. Multi layer face-down or edge-up oriented active layers of CQWs could be a topic of further investigation. One can also approach to the subject as the combinations of edge-up and face-down oriented colloidal quantum wells as the active layer of LS-NS devices.

What is more remarkable would be the numerical study on the Eq. **2.1.1**. Since LS-NS devices work on the principle of photovoltage build-up, they can also be utilized as a characterization tool of metal-semiconductor contacts, specially for semiconductor nanocrystals, with the help of numerical characterizations of the photovoltage build-up.

Since no electrical driving is used for photovoltage build-up, it could theoretically bypass possible problems, like short circuiting or parallel currents which could possibly mislead the measurements. If a dedicated study takes place to interconnect the term of rate of generation in the Eq. **2.1.1**, and the amount of photogenerated excitons, it could possibly be used to achieve a deeper understanding of the nature of charge transport between metal-semiconductor contacts of colloidal quantum wells.

Bibliography

[1] H. Schneider, Quantum Well Infrared Photodetectors, Berlin: Springer Berlin, Heidelberg, 2007, pp. 5-12.

[2] Michel, J., Liu, J., & Kimerling, L. C. (2010). High-performance Ge-on-Si photodetectors. Nature Photonics, 4(8), 527–534. https://doi.org/10.1038/nphoton.2010.157.

[3] Balagurov, L. A., Bayliss, S. C., Andrushin, S. Y., Orlov, A. F., Ünal, B., Yarkin, D. G., & Petrova, E. A. (2001). Metal/PS/c-Si photodetectors based on unoxidized and oxidized porous silicon. *Solid-state Electronics*, *45*(9), 1607–1611. https://doi.org/10.1016/s0038-1101(01)00154-x

[4] Dai, X., Zhang, S., Wang, Z., Adamo, G., Liu, H., Huang, Y., Couteau, C., & Soci, C. (2014). GaAs/AlGaAs Nanowire Photodetector. *Nano Letters*, *14*(5), 2688–2693. https://doi.org/10.1021/nl5006004

[5] Megherbi, D. B., Paradiso, G., Vakil, I., Limberopoulos, N. I., & Urbas, A. (2015). *A wavelet de-noising signal processing method for overall noise-to-signal (NSR) profile extraction, characterization and comparison of 3μm-5μm MWIR strained-layer super-lattice (SLS) photo-detectors enhanced with microsphere lenses of different material structures and sizes*. https://doi.org/10.1109/naecon.2015.7443054

[6] Herzinger, C. M., Johs, B., McGahan, W. A., Woollam, J. A., & Paulson, W. M. (1998). Ellipsometric determination of optical constants for silicon and thermally grown silicon dioxide via a multi-sample, multi-wavelength, multi-angle investigation. *Journal of Applied Physics*, *83*(6), 3323–3336. https://doi.org/10.1063/1.367101

[7] Zulehner, W. (1983). Czochralski growth of silicon. *Journal of Crystal Growth*, *65*(1–3), 189–213. https://doi.org/10.1016/0022-0248(83)90051-9

[8] Bauhuis, G., Mulder, P. G., Haverkamp, E., Huijben, J. B., & Schermer, J. J. (2009). 26.1% thin-film GaAs solar cell using epitaxial lift-off. *Solar Energy Materials and Solar Cells*, *93*(9), 1488–1491. https://doi.org/10.1016/j.solmat.2009.03.027

[9] Erdem, O., Gungor, K., Guzelturk, B., Tanriover, I., Sak, M., Olutas, M., Dede, D. S., Kelestemur, Y., & Demir, H. V. (2019). Orientation-Controlled Nonradiative Energy Transfer to Colloidal Nanoplatelets: Engineering Dipole Orientation Factor. *Nano Letters*, *19*(7), 4297–4305. https://doi.org/10.1021/acs.nanolett.9b00681

[10] Erdem, O., Foroutan, S., Gheshlaghi, N., Guzelturk, B., Altintas, Y., & Demir, H. V. (2020). Thickness-Tunable Self-Assembled Colloidal Nanoplatelet Films Enable Ultrathin Optical Gain Media. *Nano Letters*, *20*(9), 6459–6465. https://doi.org/10.1021/acs.nanolett.0c02153

[11] Baruj, H. D., Bozkaya, I., Canimkurbey, B., Isik, A. T., Shabani, F., Delikanli, S., Shendre, S., Erdem, O., Isik, F., & Demir, H. V. (2023). Highly-Directional, Highly-Efficient Solution-Processed Light-Emitting Diodes of All-Face-Down Oriented Colloidal Quantum Well Self-Assembly. *Small*. https://doi.org/10.1002/smll.202206582

[12] Yeltik, A., Delikanli, S., Olutas, M., Kelestemur, Y., Guzelturk, B., & Demir, H. V. (2015). Experimental Determination of the Absorption Cross-Section and Molar Extinction Coefficient of Colloidal CdSe Nanoplatelets. *Journal of Physical Chemistry C*, *119*(47), 26768–26775. https://doi.org/10.1021/acs.jpcc.5b09275

[13] Akhavan, S., Guzelturk, B., Sharma, V., & Demir, H. V. (2012). Large-area semi-transparent light-sensitive nanocrystal skins. *Optics Express*, *20*(23), 25255. https://doi.org/10.1364/oe.20.025255

[14] Barbagiovanni, E. G., Lockwood, D. J., Simpson, P. T., & Goncharova, L. V. (2014). Quantum confinement in Si and Ge nanostructures: Theory and experiment. *Applied Physics Reviews*, *1*(1), 011302. https://doi.org/10.1063/1.4835095

[15] Ithurria, S., Tessier, M. D., Mahler, B., Lobo, R. P. S. M., Dubertret, B., & Efros, A. L. (2011). Colloidal nanoplatelets with two-dimensional electronic structure. *Nature Materials*, *10*(12), 936–941. https://doi.org/10.1038/nmat3145

[16] Thorkelsson, K., Bai, P., & Xu, T. (2015). Self-assembly and applications of anisotropic nanomaterials: A review. *Nano Today*, *10*(1), 48–66. https://doi.org/10.1016/j.nantod.2014.12.005

[17] Zhuge, F., Zheng, Z., Luo, P., Lv, L., Huang, Y., Li, H., & Zhai, T. (2017). Nanostructured Materials and Architectures for Advanced Infrared Photodetection. *Advanced Materials and Technologies*, *2*(8), 1700005. https://doi.org/10.1002/admt.201700005

[18] Chetia, A., Bera, J., Betal, A., & Sahu, S. (2022). A brief review on photodetector performance based on zero dimensional and two dimensional materials and their hybrid structures. *Materials Today Communications*, *30*, 103224. https://doi.org/10.1016/j.mtcomm.2022.103224

[19] Akhavan, S., Cihan, A., Bozok, B., & Demir, H. V. (2014). Nanocrystal Skins with Exciton Funneling for Photosensing. *Small*, *10*(12), 2470–2475. https://doi.org/10.1002/smll.201303808

[20] Akhavan, S., Gungor, K., Mutlugun, E., & Demir, H. V. (2013). Plasmonic light-sensitive skins of nanocrystal monolayers. *Nanotechnology*, *24*(15), 155201. https://doi.org/10.1088/0957-4484/24/15/155201

[21] Akhavan, S., Uran, C., Bozok, B., Gungor, K., Kelestemur, Y., Lesnyak, V., Gaponik, N., Eychmüller, A., & Demir, H. V. (2016). Flexible and fragmentable tandem photosensitive nanocrystal skins. *Nanoscale*, *8*(8), 4495–4503. https://doi.org/10.1039/c5nr05063d

[22] Eisler, H., Sundar, V. C., Bawendi, M. G., Walsh, M., Smith, H. I., & Klimov, V. I. (2002). Color-selective semiconductor nanocrystal laser. *Applied Physics Letters*, *80*(24), 4614–4616. https://doi.org/10.1063/1.1485125

[23] Schaller, R., Petruska, M. A., & Klimov, V. I. (2003). Tunable Near-Infrared Optical Gain and Amplified Spontaneous Emission Using PbSe Nanocrystals. *Journal of Physical Chemistry B*, *107*(50), 13765–13768. https://doi.org/10.1021/jp0311660

[24] Manna, L., Milliron, D. J., Meisel, A., Scher, E. C., & Alivisatos, A. P. (2003). Controlled growth of tetrapod-branched inorganic nanocrystals. *Nature Materials*, *2*(6), 382–385. https://doi.org/10.1038/nmat902

[25] Joo, J. C., Son, J. S., Kwon, S. Y., Yu, J., & Hyeon, T. (2006). Low-Temperature Solution-Phase Synthesis of Quantum Well Structured CdSe Nanoribbons. *Journal of the American Chemical Society*, *128*(17), 5632–5633. https://doi.org/10.1021/ja0601686

[26] Pietryga, J. M., Schaller, R. D., Werder, D. J., Stewart, M. G., Klimov, V. I., & Hollingsworth, J. A. (2004). Pushing the Band Gap Envelope: Mid-Infrared Emitting Colloidal PbSe Quantum Dots. *Journal of the American Chemical Society*, *126*(38), 11752–11753. https://doi.org/10.1021/ja047659f

[27] Murray, C. D., Kagan, C. R., & Bawendi, M. G. (2000). Synthesis and Characterization of Monodisperse Nanocrystals and Close-Packed Nanocrystal Assemblies. *Annual Review of Materials Science*, *30*(1), 545–610. https://doi.org/10.1146/annurev.matsci.30.1.545

[28] Kim, S. W., Fisher, B., Eisler, H., & Bawendi, M. G. (2003). Type-II Quantum Dots: CdTe/CdSe(Core/Shell) and CdSe/ZnTe(Core/Shell) Heterostructures. *Journal of the American Chemical Society*, *125*(38), 11466–11467. https://doi.org/10.1021/ja0361749

[29] Hines, M. A., & Guyot-Sionnest, P. (1996). ChemInform Abstract: Synthesis and Characterization of Strongly Luminescing ZnS-Capped CdSe Nanocrystals. *ChemInform*. https://doi.org/10.1002/chin.199619004

[30] Park, Y., Roh, J., Diroll, B. T., Schaller, R. D., & Klimov, V. I. (2021). Colloidal quantum dot lasers. *Nature Reviews Materials*, *6*(5), 382–401. https://doi.org/10.1038/s41578-020-00274-9

[31] Garcia-Santamaria, F., Chen, Y., Vela, J., Schaller, R. D., Hollingsworth, J. A., & Klimov, V. I. (2009). Suppressed Auger Recombination in "Giant" Nanocrystals Boosts Optical Gain Performance. *Nano Letters*, *9*(10), 3482–3488. https://doi.org/10.1021/nl901681d

[32] Kunneman, L. T., Tessier, M. D., Heuclin, H., Dubertret, B., Aulin, Y. V., Grozema, F. C., Schins, J. M., & Siebbeles, L. D. A. (2013). Bimolecular Auger

Recombination of Electron–Hole Pairs in Two-Dimensional CdSe and CdSe/CdZnS Core/Shell Nanoplatelets. *Journal of Physical Chemistry Letters*, *4*(21), 3574–3578. https://doi.org/10.1021/jz401970p

[33] Delikanli, S., Erdem, O., Isik, F., Baruj, H. D., Shabani, F., Yagci, H. B., Durmusoglu, E. G., & Demir, H. V. (2021). Ultrahigh Green and Red Optical Gain Cross Sections from Solutions of Colloidal Quantum Well Heterostructures. *American Chemical Society*, *12*(9), 2177–2182. https://doi.org/10.1021/acs.jpclett.0c03836

[34] She, C., Fedin, I., Dolzhnikov, D. S., Demortière, A., Schaller, R. D., Pelton, M., & Talapin, D. V. (2014). Low-Threshold Stimulated Emission Using Colloidal Quantum Wells. *Nano Letters*, *14*(5), 2772–2777. https://doi.org/10.1021/nl500775p

[35] Diroll, B. T. (2020). Colloidal quantum wells for optoelectronic devices. *Journal of Materials Chemistry C*, *8*(31), 10628–10640. https://doi.org/10.1039/d0tc01164a

[36] Akhavan, S., Yeltik, A., & Demir, H. V. (2014). Photosensitivity Enhancement with TiO2 in Semitransparent Light-Sensitive Skins of Nanocrystal Monolayers. *ACS Applied Materials & Interfaces*, *6*(12), 9023–9028. https://doi.org/10.1021/am502472y

[37] Akhavan, S., Akgul, M. Z., Hernandez-Martinez, P. L., & Demir, H. V. (2017). Plasmon-Enhanced Energy Transfer in Photosensitive Nanocrystal Device. *ACS Nano*, *11*(6), 5430–5439. https://doi.org/10.1021/acsnano.6b08392

[38] Akhavan, S., Cihan, A., Yeltik, A., Bozok, B., Lesnyak, V., Gaponik, N., Eychmüller, A., & Demir, H. V. (2016). Multiexciton generation assisted highly photosensitive CdHgTe nanocrystal skins. *Nano Energy*. https://doi.org/10.1016/j.nanoen.2016.04.055

[39] Bertrand, G., Polovitsyn, A., Christodoulou, S., Khan, A. R., & Moreels, I. (2016). Shape control of zincblende CdSe nanoplatelets. *Chemical Communications*, *52*(80), 11975–11978. https://doi.org/10.1039/c6cc05705e

[40] Olutas, M., Guzelturk, B., Kelestemur, Y., Yeltik, A., Delikanli, S., & Demir, H. V. (2015). Lateral Size-Dependent Spontaneous and Stimulated Emission Properties in Colloidal CdSe Nanoplatelets. *ACS Nano*, *9*(5), 5041–5050. https://doi.org/10.1021/acsnano.5b01927

[41] Uda, T., Yoshida, M., Ishii, A., & Kato, Y. (2016). Electric-Field Induced Activation of Dark Excitonic States in Carbon Nanotubes. *Nano Letters*, *16*(4), 2278–2282. https://doi.org/10.1021/acs.nanolett.5b04595

[42] Singh, S., Tomar, R., Brinck, S. T., De Roo, J., Geiregat, P., Martins, J. C., Infante, I., & Hens, Z. (2018). Colloidal CdSe Nanoplatelets, A Model for Surface Chemistry/Optoelectronic Property Relations in Semiconductor Nanocrystals. *Journal of the American Chemical Society*, *140*(41), 13292–13300. https://doi.org/10.1021/jacs.8b07566

[43] Bozkaya, T., Isik, F., Bozkaya, I., Delikanli, S., Demir, H. V. Light-Sensitive Monolayer-Thick Nanocrystal Skins of Face-Down Self-Oriented Colloidal Quantum Wells. (in submission)